Statistics

The results are presented as the mean ± SE of the mean. Comparisons among the three groups were evaluated by one-way analysis of variance followed by Scheffe's post hoc test. Statistical significance was defined as $p < .05$.

Results

Significant Engraftment of a Single Tip-SP CD34⁻KSL Cell

Either TBM cells (1×10^6, TBM group), c-Kit⁺, Sca-1⁺, Lin⁻ cells (3×10^3, KSL fraction), or a single Tip-SP CD34⁻KSL cell (1, HSC fraction) were injected into lethally irradiated wild-type mice. Consistent with our previous report [2], a single Tip-SP CD34⁻KSL cell showed significant donor cell engraftment for long term (Figs. 1A, 1B). Consistent with our previous study [2], both myelocytes/monocytes and T/B lymphocytes derived from a single Tip-SP cell were detected at 3, 6, and 12 months after transplantation. Flow cytometry at 16 weeks after bone marrow reconstitution revealed that peripheral blood cells had been reconstituted with the injected cells in TBM (79.6% ± 5.1%), KSL (68.4% ± 5.1%), and HSC (34.4% ± 6.5%) groups (Fig. 1B).

Failure of a Single HSC-Derived Cell to Participate in Vascular Remodeling

Wire-mediated endovascular injury was induced to the femoral artery at 12 weeks after irradiation and injection. At 16 weeks after stem cell transplantation, the femoral arteries showed neointimal formation that mainly consisted of α-SMA–positive cells in all groups (Fig. 2A). The neointima contained a significant number of GFP-positive cells in the TBM group (24.0% ± 7.2%; $n = 4$) and the KSL group (14.1% ± 6.1%; $n = 6$). On the other hand, GFP-positive cells were seldom detected in the neointima of the HSC group (0.2% ± 0.1%; $n = 7$). Similarly, the media contained a significant number of GFP-positive cells in the TBM group (31.1% ± 11.2%) and KSL group (16.8% ± 6.6%). In contrast, GFP-positive cells were rarely detected in the media in the HSC group (2.7% ± 1.0%) (Fig. 2B, Table 1).

Next, we characterized the bone marrow–derived cells observed in the vascular lesions. In the KSL group as well as in the TBM group, many GFP-positive cells expressed α-SMA in the neointima and media (Figs. 3A–3C). The bone marrow–derived cells on the luminal side were positive for endothelial markers (BS-lectin and CD31) (Figs. 3D, 3E), as previously reported [7]. In the HSC group, very few GFP-positive cells were detected in the lesions in the HSC group (Fig. 3C). All of the GFP-positive cells were positive for CD45 (Fig. 3F). We could not find GFP-positive cells that expressed α-SMA or endothelial markers.

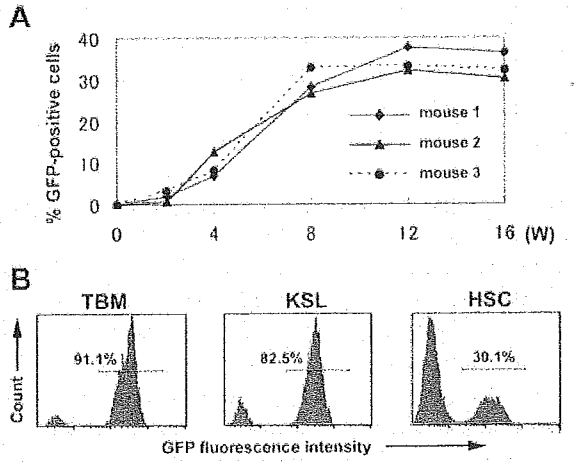

Figure 1. Successful engraftment of a single Tip-SP CD34⁻KSL cell, 1×10^6 total bone marrow (TBM group) cells ($n = 4$), 3×10^3 c-Kit⁺ Sca-1⁺ Lin⁻ (KSL group) fraction cells ($n = 6$), or a single Tip-SP CD34⁻KSL cell (HSC group) ($n = 7$) harboring green fluorescent protein (GFP) were injected into lethally irradiated wild-type mice. **(A):** Proportion of the GFP-positive cells in peripheral blood after transplantation of a single Tip-SP CD34⁻KSL cell. Time courses of three representative mice are reported. **(B):** Representative flow cytometric histograms of peripheral leukocytes in TBM, KSL, and HSC groups at 16 weeks after transplantation. Abbreviations: HSC, hematopoietic stem cell; SP, side population.

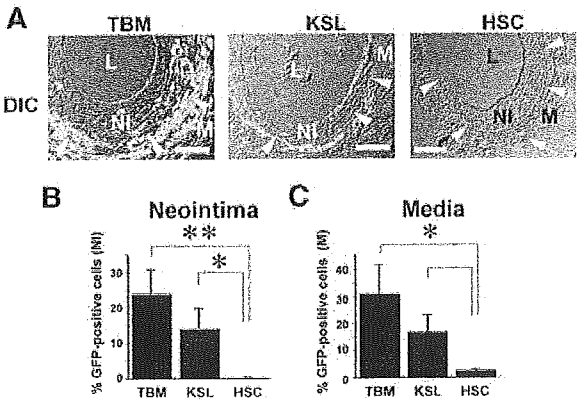

Figure 2. Failure of a highly purified HSC to contribute to vascular remodeling after mechanical vascular injury. **(A):** Representative cross-sections of the vascular lesions. At 12 weeks after irradiation and stem cell transplantation, wire-mediated injury was induced in the femoral artery of the bone marrow chimeric mice. The injured arteries were harvested at 16 weeks, embedded in plastic resin, and observed under a confocal microscope (FLUOVIEW FV300; Olympus). Arrowheads indicate the internal elastic lamina. Arrow indicates a GFP-positive cell observed in adventitia in the HSC group. Bar = 50 μm. **(B, C):** Frequency of GFP-positive cells among the total cells in the **(B)** neointima and **(C)** media. *$p < .05$; **$p < .01$. Abbreviations: DIC, differential interference contrast; GFP, green fluorescent protein; HSC, hematopoietic stem cell; KSL, c-Kit⁺, Sca-1⁺, Lineage⁻; L, lumen; M, media; NI, neointima; TBM, total bone marrow.

Table 1. Frequency of green fluorescent protein (GFP)–positive cells in neointima and media per a cross-section 4 weeks after vascular injury in bone marrow chimeric mice

	Neointima	Media
	No. of GFP$^+$ cells/ no. of total cells per a cross-section	No. of GFP$^+$ cells/ no. of total cells per a cross-section
TBM group		
Mouse 1	162/406	48/81
Mouse 2	17/237	10/51
Mouse 3	104/339	45/120
Mouse 4	42/231	11/138
KSL group		
Mouse 1	89/209	22/53
Mouse 2	19/109	15/46
Mouse 3	4/150	3/69
Mouse 4	7/58	2/104
Mouse 5	10/145	14/133
Mouse 6	10/319	5/49
HSC group		
Mouse 1	0/291	1/44
Mouse 2	0/73	1/13
Mouse 3	0/210	1/24
Mouse 4	0/362	0/24
Mouse 5	0/235	0/68
Mouse 6	1/162	1/37
Mouse 7	1/104	1/42

Wire-mediated endovascular injury was induced in the femoral arteries of marrow chimeric mice, which received either total bone marrow cells (1×10^6, TBM group), c-Kit$^+$, Sca-1$^+$, Lineage$^-$ cells (3×10^3, KSL group), or highly purified hematopoietic stem cell (1, HSC group). The injured arteries were harvested 4 weeks after vascular injury and embedded in plastic resin. After counterstaining with Hoechst 33258, sections were observed under a fluorescence microscope. Cell number was counted in the neointima and media of a cross-section of each artery.

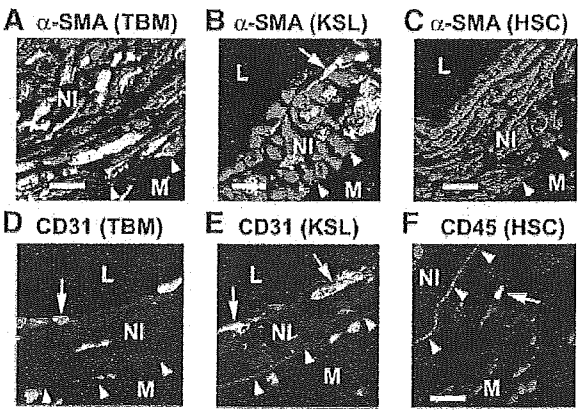

Figure 3. Double immunofluorescent images of the injured arteries. Plastic-embedded sections were stained for (**A, B, C**) α-smooth muscle actin (α-SMA, red), (**D, E**) CD31 (red), and (**F**) CD45 (red) followed by counterstaining with Hoechst 33258 (blue). Arrowheads indicate the internal elastic lamina. Arrows indicate green fluorescent protein–positive cells that were positive for markers. Bar = 10 μm. Abbreviations: HSC, hematopoietic stem cell; KSL, c-Kit$^+$, Sca-1$^+$, Lineage$^-$; L, lumen; M, media; NI, neointima; TBM, total bone marrow.

Discussion

The present study was designed to rigorously determine the plasticity of an HSC in vivo by analyzing the vascular lesions induced by wire injury after bone marrow reconstitution with a single HSC. Although a single HSC showed an appreciable level of hematopoietic engraftment activity, very few cells in the lesion were derived from the single HSC. In contrast, the GFP-positive cells substantially contributed to vascular remodeling when bone marrow was reconstituted with TBM cells or KSL cells [7, 11].

The HSCs used in this study had the strongest dye-efflux activity with nearly complete level of hematopoietic engraftment activity [2]. We could detect the single Tip-SP CD34-KSL–derived cells not only in T/B lymphocytes but also in myeloid lineage even at 12 months after transplantation [2]. Given the short life of mature myeloid cells, the long-term chimerism in total hematopoietic cells supports the notion that the single Tip-SP CD34-KSL cell undergoes self-renewal and continuously gives rise to progenitors of T/B lymphocytes and myelocytes/monocytes. Moreover, the Tip-SP CD34-KSL cells are homogenous in size and morphology as determined by flow cytometric analysis of 10,000 Tip-SP CD34-KSL cells [2]. About 90% of the Tip-SP CD34-KSL cells can form huge colonies in colony assay (Y. Matsuzaki, unpublished observations). We assume that the diverse chimerism results from the difference in place where the transplanted Tip-SP CD34-KSL cell homes.

Our result suggests that it is rare for a highly purified HSC to transdifferentiate into vascular cells. In contrast, the KSL fraction of bone marrow cells contained a distinct population that could substantially contribute to lesion formation. Although the KSL fraction is considered to be enriched in HSCs [4], mesenchymal stem cells or multipotent cells that are more primitive than HSCs [14] could be included in this fraction. It is plausible that those nonhematopoietic cells in the KSL fraction might be responsible for the KSL-derived endothelial-like cells or smooth muscle–like cells observed in the vascular lesion.

Recent reports suggest that HSCs adopt tissue-specific phenotype by cell fusion but not by transdifferentiation [15]. Previous reports documented polyploidization of vascular smooth muscle cells in response to mechanical and humoral stimuli [16]. Thus, it is possible that cell fusion can account for, at least in part, the accumulation of bone marrow–derived smooth muscle–like cells in vascular lesions. However, we seldom detected the HSC-derived cells in the vascular lesions. It would be rare for an HSC to contribute to vascular remodeling even by cell fusion.

Conclusion

Our finding suggests that a highly purified murine HSC seldom transdifferentiates into vascular cells. Distinct cell populations other than hematopoietic cells may be responsible for most bone marrow–derived smooth muscle–like cells and endothelial like–cells that could be observed in vascular lesions after mechanical injury.

Acknowledgments

This study was supported in part by grants from the Japanese Ministry of Education, Culture, Sports, Science, and Technology and from the Japanese Ministry of Health, Labor, and Welfare.

References

1 Poulsom R, Alison MR, Forbes SJ et al. Adult stem cell plasticity. J Pathol 2002;197:441–456.

2 Matsuzaki Y, Kinjo K, Mulligan RC et al. Unexpectedly efficient homing capacity of purified murine hematopoietic stem cells. Immunity 2004;20:87–93.

3 Krause DS, Theise ND, Collector MI et al. Multi-organ, multi-lineage engraftment by a single bone marrow-derived stem cell. Cell 2001;105:369–377.

4 Lagasse E, Connors H, Al-Dhalimy M et al. Purified hematopoietic stem cells can differentiate into hepatocytes in vivo. Nat Med 2000;6:1229–1234.

5 Jang YY, Collector MI, Baylin SB et al. Hematopoietic stem cells convert into liver cells within days without fusion. Nat Cell Biol 2004;6:532–539.

6 Orlic D, Kajstura J, Chimenti S et al. Bone marrow cells regenerate infarcted myocardium. Nature 2001;410:701–705.

7 Sata M, Saiura A, Kunisato A et al. Hematopoietic stem cells differentiate into vascular cells that participate in the pathogenesis of atherosclerosis. Nat Med 2002;8:403–409.

8 Wagers AJ, Sherwood RI, Christensen JL et al. Little evidence for developmental plasticity of adult hematopoietic stem cells. Science 2002;297:2256–2259.

9 Osawa M, Hanada K, Hamada H et al. Long-term lymphohematopoietic reconstitution by a single CD34-low/negative hematopoietic stem cell. Science 1996;273:242–245.

10 Blau H, Brazelton T, Keshet G et al. Something in the eye of the beholder. Science 2002;298:361–362.

11 Tanaka K, Sata M, Hirata Y et al. Diverse contribution of bone marrow cells to neointimal hyperplasia after mechanical vascular injuries. Circ Res 2003;93:783–790.

12 Okada S, Yoshida T, Hong Z et al. Impairment of B lymphopoiesis in precocious aging (klotho) mice. Int Immunol 2000;12:861–871.

13 Sata M, Maejima Y, Adachi F et al. A mouse model of vascular injury that induces rapid onset of medial cell apoptosis followed by reproducible neointimal hyperplasia. J Mol Cell Cardiol 2000;32:2097–2104.

14 Jiang Y, Jahagirdar BN, Reinhardt RL et al. Pluripotency of mesenchymal stem cells derived from adult marrow. Nature 2002;418:41–49.

15 Vassilopoulos G, Wang PR, Russell DW. Transplanted bone marrow regenerates liver by cell fusion. Nature 2003;422:901–904.

16 Campbell JH, Tachas G, Black MJ et al. Molecular biology of vascular hypertrophy. Basic Res Cardiol 1991;86:3–11.

Histopathology 2005, 47, 348–356. DOI: 10.1111/j.1365-2559.2005.02223.x

Expression of a candidate marker for progenitor cells, Musashi-1, in the proliferative regions of human antrum and its decreased expression in intestinal metaplasia

Y Akasaka, Y Saikawa,[1] K Fujita, T Kubota,[1] Y Ishikawa, A Fujimoto, T Ishii, H Okano[2] & M Kitajima[1]

Department of Pathology, School of Medicine, Toho University, [1]Department of Surgery and [2]Department of Physiology, Keio University School of Medicine, Tokyo, Japan

Date of submission 11 December 2004
Accepted for publication 15 March 2005

Akasaka Y, Saikawa Y, Fujita K, Kubota T, Ishikawa Y, Fujimoto A, Ishii T, Okano H & Kitajima M (2005) *Histopathology* 47, 348–356

Expression of a candidate marker for progenitor cells, Musashi-1, in the proliferative regions of human antrum and its decreased expression in intestinal metaplasia

Aim: Reliable makers for progenitor cells in the human stomach have not been elucidated. The aim of the present study was to clarify whether Musashi-1 (Msi-1), which has recently been proposed as a stem cell marker in mouse intestine, serves as a marker for progenitor cells in human stomach.

Methods and results: Immunohistochemistry revealed that Msi-1+ cells were detected especially in the isthmus/neck region (the putative position of stem cells) of the adult antrum, but were limited to the basal regions of fetal pyloric glands during the early stages of development. These results suggest that Msi-1 expression occurs specifically in the stem cell-containing regions. Msi-1+ cells were intermingled with proliferating cell nuclear antigen (PCNA)+ cells in the isthmus/neck region of the adult antrum, but did not coexpress PCNA or Ki67. Msi-1 expression overlapped partly with expression of MUC5AC and MUC6, indicating that Msi-1+ cells retain some features of both foveolar and pyloric gland cell differentiation phenotypes. In contrast, Msi-1 expression in gastric glands showing intestinal metaplasia (IM) became weaker than that in the glands without IM.

Conclusion: The specific expression of Msi-1 within the proliferative regions suggests that Msi-1 is a marker of cells with progenitor characteristics before active proliferation in human antrum.

Keywords: gastric-type mucins, Msi-1, progenitor cell, proliferation, stomach

Abbreviations: H&E, haematoxylin and eosin; IM, intestinal metaplasia; Msi-1, Musashi-1; PBS, phosphate-buffered saline; PCNA, proliferating cell nuclear antigen; SDS, sodium dodecyl sulphate; TBS, Tris-buffered saline

Introduction

The epithelium of the adult stomach possesses a cell renewal system in which stem cells, thought to be present in the proliferative region of the isthmus/neck of the glands, differentiate into the surface mucous epithelial and glandular cells.[1–6] During this process, the immediate descendants derived from the stem cells undergo a complex bipolar migration from the neck/isthmus region, moving either upward or downward.[7,8] Indeed, in the mouse stomach, all three types of progenitor cells (prepit, preneck, and preparietal cells) have been found to originate from multipotential granule-free cells in the isthmus region.[9] However, the lack of useful markers has made it difficult to characterize the progenitor cells in the human stomach and has hindered the study of their origin.[10]

The Musashi family is an evolutionarily conserved group of neural RNA-binding proteins that has representatives in *Drosophila melanogaster*, mice and humans.[11–13] The mammalian homolog, Musashi-1

Address for correspondence: Yoshikiyo Akasaka, Department of Pathology, School of Medicine, Toho University, 5-21-16 Omori-nishi, Ohta City, Tokyo 143–8540, Japan.
e-mail: akasakay@med.toho-u.ac.jp

(Msi-1), is selectively expressed in neural progenitor cells, including neural stem cells.[14] Although its precise functions have not yet been clarified, Msi-1 is thought to be involved in the early asymmetric divisions that generate differentiated cells from neural stem cells. Interestingly, Msi-1 expression has also been identified outside the nervous system.[15,16] Specifically, it has been shown that Msi-1 is preferentially expressed in the predicted stem cell regions of murine and human intestinal crypts, suggesting that Msi-1 may be a marker for intestinal stem cells and their immediate descendants.[15,16] By analogy, stem cells are presumed to exist in human gastric glands and therefore it would be expected that Msi-1 is expressed in the glands.[4,10] In the present study, to clarify whether Msi-1 is expressed in the putative stem cells or progenitor cells in human gastric glands as in the murine intestine, we examined the expression profile of Msi-1 in the normal human stomach and compared it with those of proliferative antigens [proliferating cell nuclear antigen (PCNA) and Ki67] and gastric-type mucins (MUC5AC and MUC6).

Materials and methods

TISSUE SAMPLES

Thirty-three surgically resected non-cencerous gastric specimens were selected from the archives of the Department of Pathology, Hiratsuka City Hospital, Kanagawa, Japan. These had originally been obtained from 33 patients (aged 40–68 years) during surgery for duodenal ulcers or pancreatic tumours.

The fetal stomach was studied using gastric specimens removed at autopsy from two fetuses in the 14th week of gestation, two in the 19th week, three in the 22nd week, and three in the 27th week. Only well-preserved gastric specimens were used.

To examine the levels of Msi-1 expression in intestinal metaplasia (IM), 62 human stomach tissue samples were selected from biopsy specimens of IM mucosa (31 of incomplete IM type and 31 of complete IM type) from 62 patients (aged 36–72 years) at the Toho University School of Medicine. After a section from each sample was stained with haematoxylin and eosin (H&E), IM was classified as complete or incomplete according to previously described histological criteria: tissue of the complete type contains goblet cells and Paneth cells, whereas tissue of the incomplete type is devoid of Paneth cells.[17] Fully informed consent was obtained from all the adult subjects and the parents of the fetuses. All human materials examined in this study were treated in accordance with the guidelines of the Helsinki Declaration of 1975, as revised in 1983.

IMMUNOHISTOCHEMISTRY

The Msi-1 antibody that we used (14H1) is a rat monoclonal antibody that recognizes amino acids 235–244 of Msi-1.[14] This region is conserved in Xenopus, mouse and human. The antibody does not cross-react with a related protein, Musashi-2.[16] Immunostaining for Msi-1 was performed as described previously.[18] In brief, the sections were treated with 3% H_2O_2 in 0.1 M phosphate-buffered saline (PBS) for 10 min, then incubated with the Msi-1 antibody (diluted to a final concentration of 1 μg/ml) at 4°C overnight.[14] After incubation with a biotinylated goat anti-rat antibody (Dako, Glostrup, Denmark) for 1 h, the sections were washed with PBS and further incubated with streptavidin–biotin–peroxidase complex (Dako) for 40 min. The reaction products were stained with a 0.02% solution of 3,3′-diaminobenzidine in 0.05 M Tris–HCl buffer (pH 7.2) containing 0.01% H_2O_2. Slides were counterstained with haematoxylin, dehydrated and mounted. The negative control was incubated with an immunoglobulin from rat at the same final concentration, but without the primary antibody. The extent of Msi-1+ IM cells was estimated semiquantitatively according to the percentage of stained cells among the total number of IM cells in each biopsy tissue section. The percentage of positive cells was divided into four grades; 0 (absent), 1 (< 20% of cells positive), 2 (20–50% of cells positive), and 3 (> 50% of the cells positive).

DOUBLE-LABELLING

The combinations used in the immunohistochemical double-labelling were rat anti-mouse Msi-1 antibody plus either mouse anti-human PCNA (dilution 1 : 100; Dako), Ki67 (1 : 50; Dako), MUC5AC (1 : 100; Zymed Laboratories, South San Francisco, CA, USA), MUC6 (NCL-MUC-6, 1 : 50; Novocastra, Newcastle, UK) or TFF1 (pS2, 1 : 100; Zymed) antibody as the primary antibodies, and biotinylated goat anti-rat antibody (Dako) plus alkaline phosphatase-conjugated goat anti-mouse antibody (Dako) as the secondary antibodies.[19] The sections were treated with alkaline phosphatase substrate solution (New fuchsin substrate system; Dako) to develop the alkaline phosphatase and allow visualization of the antigens.

The combination used in immunofluorescent double-labelling was rat anti-mouse Msi-1 antibody plus mouse anti-human PCNA antibody (1 : 100; Dako) as the primary antibodies, and Texas red-conjugated rabbit anti-rat antibody (Vector Laboratories, Ontario, Canada) plus fluorescein-conjugated horse anti-mouse antibody (Vector) as the secondary antibodies.[20] The

images were captured by confocal microscopy using a BioRad RADIANCE 2100 laser scanning system (Bio-Rad, Hercules, CA, USA).

WESTERN BLOT ANALYSIS

Frozen stomach tissue samples were obtained from one of the 33 surgically resected stomachs described above. For detection of the Msi-1 protein by immunoblotting, the tissue samples were homogenized in radio-immunoprecipitation assay lysis buffer [1% Nonidet P-40, 0.1% sodium dodecyl sulphate (SDS), 100 μg/ml phenylmethyl sulfonyl fluoride (PMSF), 0.5% sodium deoxycholate, 1 mM sodium orthovanadate, 2 μg/ml aprotinin, 2 μg/ml antipain, and 2 μg/ml leupeptin in PBS] on ice, and after centrifugation at 13 000 *g* at 4°C for 20 min, the supernatants were collected.[21] Protein concentration was determined by using the Bradford assay (BioRad), and tissue lysates were mixed with an equal amount of 2 × SDS loading buffer (100 mM Tris–HCl, 4% SDS, 20% glycerol, and 0.2% bromophenol blue), as described previously.[22] Samples were heated at 100°C for 5–10 min before loading and separated on 12% SDS–polyacrylamide gels (BioRad). The proteins were electrotransferred to a nitrocellulose membrane (Amersham, Arlington Heights, IL, USA) in transfer buffer containing 48 mM Tris–HCl, 39 mM glycine, 0.037% SDS, and 20% methanol at 4°C for 1 h. Non-specific binding to the membrane was blocked for 1 h at room temperature with 5% Carnation non-fat milk in Tris-buffered saline (TBS) buffer (20 mM Tris–HCl, 150 mM NaCl, and 0.1% Tween 20). The membranes were then incubated for 16 h at 4°C with the Msi-1 antibody in blocking buffer containing 5% non-fat milk. The Msi-1 antibody was diluted to a final concentration of 1 μg/ml. Following extensive washing in TBS buffer, the membranes were incubated with a goat anti-rat IgG antibody conjugated with alkaline phosphatase (Promega, Madison, WI, USA) for 1 h at room temperature in 5% non-fat milk dissolved in TBS. Membranes were then washed with TBS buffer, and immunoreactive bands were visualized by incubation of the membrane with 5-bromo-4-chloro-3-indolyl-phosphate (BIPC)/nitroblue tetrazolium (NBT) colour substrate according to the manufacturer's protocol (Promega).

Results

Msi-1 EXPRESSION IN THE PROLIFERATIVE REGIONS OF THE ADULT HUMAN ANTRUM

In the adult human antrum, Msi-1 expression was observed predominantly in the epithelial cells of the isthmus/neck region. The cytoplasm of these epithelial cells was strongly positive for Msi-1 (Figure 1A). Many of the Msi-1+ cells were round, morphologically immature cells with a small amount of cytoplasm and a dark nucleus (Figure 1B). In contrast, the surface epithelial cells in the upper part of the pit and the epithelial cells in the basal regions of the glands were completely negative for Msi-1 expression (Figure 1A). In addition, specific expression of Msi-1 was not found in any regions of the fundic glands.

To examine the relationship between the Msi-1+ cells and the proliferative cells in the gastric glands of the human antrum, we double-stained for Msi-1 and PCNA. The proliferative regions were characterized by PCNA+ epithelial cells and were located in the isthmus/neck region. Msi-1+ cells were located mainly in the lower parts of the proliferative regions (Figure 1C). Although the Msi-1+ cells were intermingled with the PCNA+ cells in the proliferative regions, the Msi-1+ cells showed no PCNA expression, and no double-positive cells were found in any regions (Figure 1D). A further confirmatory study of immunofluorescent double-labelling for PCNA and Msi-1 using confocal laser scanning microscopy clearly demonstrated that Msi-1+ cells were not colocalized with PCNA+

Figure 1. Msi-1 expression in the proliferative regions of the adult human antrum. A, In the antral mucosa, the pits usually occupy approximately half of the mucosal thickness. Msi-1+ cells (arrow) are present in the epithelial cells of the isthmus/neck region. B, Higher magnification of the rectangular portion marked in A. Msi-1+ cells can be seen in the isthmus/neck region as round cells with small amounts of cytoplasm and dark nuclei. The arrow points to a morphologically immature cell expressing Msi-1. C, Double-staining for proliferating cell nuclear antigen (PCNA) and Msi-1 in the gastric glands of the antral mucosa. The arrows indicate PCNA+ nuclei (red labelling), which are distributed throughout the epithelial cells in the isthmus/neck region. The arrowheads indicate Msi-1+ cells (brown labelling), which are intermingled with the PCNA+ cells, are present in the lower part of the isthmus/neck region. D, Higher magnification of Msi-1+ cells within the proliferative region. Msi-1 reactivity (brown labelling) is present in the cytoplasm, while PCNA reactivity (red labelling) is restricted to the nucleus. The arrowheads indicate cells with an Msi-1+ cytoplasm but devoid of nuclear PCNA staining. The double-staining was visualized using DAB (brown labelling) and fuchsin (red labelling) substrates. E, Double-staining for PCNA and Msi-1 using confocal laser scanning microscopy. The arrows indicate cells with Msi-1+ cytoplasm (red labelling) but no nuclear PCNA staining (green labelling). The arrowheads indicate PCNA+ nuclei. F, Double-staining for Msi-1 and Ki67 in the gastric glands of the antral mucosa. The arrows indicate cells with Msi-1+ cytoplasm (brown labelling) but devoid of nuclear Ki67 staining (red labelling). The arrowheads indicate Ki67+ nuclei. The double-staining was visualized using DAB (brown labelling) and fuchsin (red labelling) substrates. Bars are 50 μm (A), 40 μm (B), 40 μm (C), 30 μm (D), 7 μm (E), and 30 μm (F).

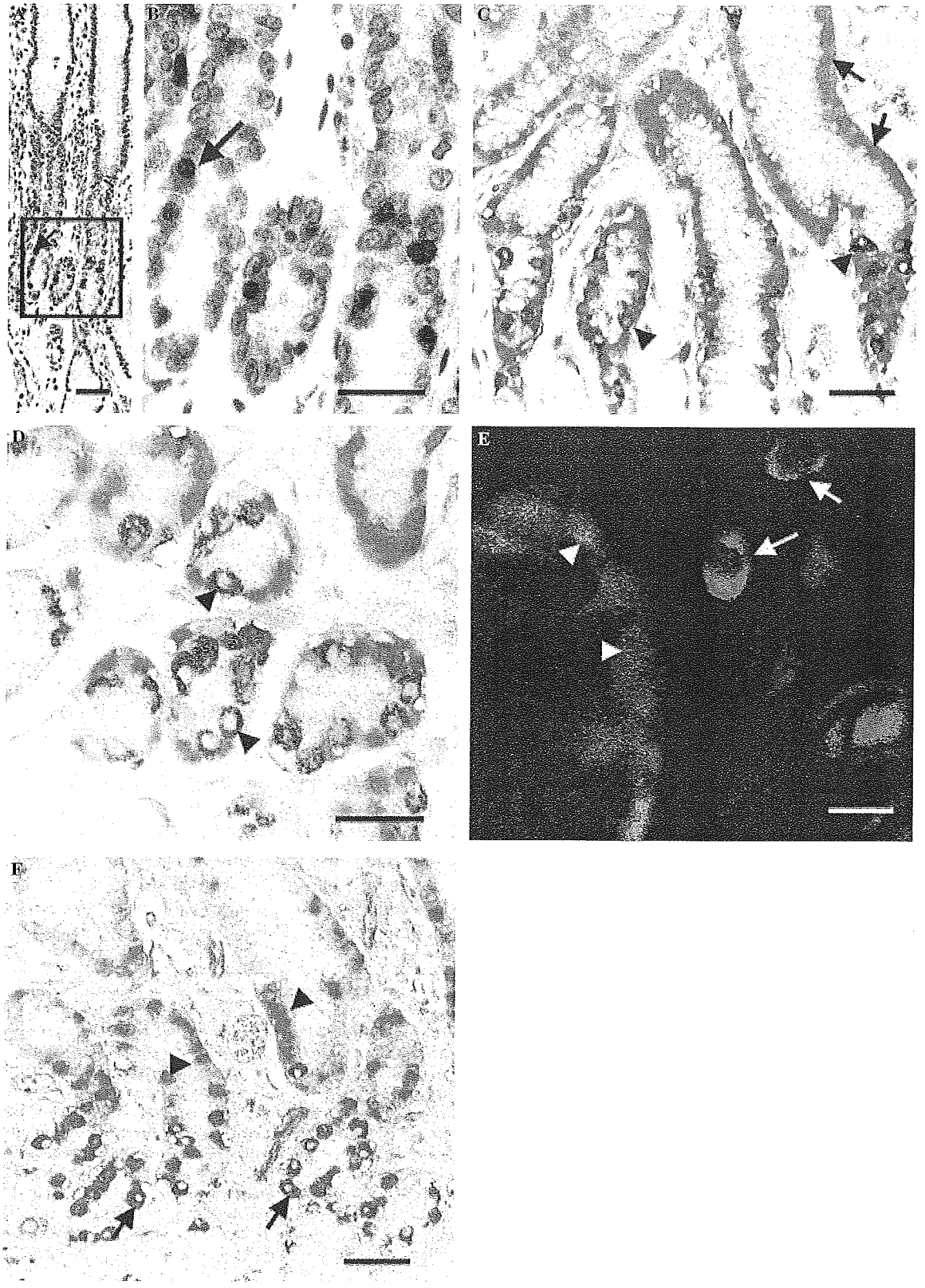

Figure 2. Western blot demonstrating the expression of Msi-1 protein in the human antrum. Frozen tissue samples from the antral, body and fundic mucosa were obtained from the same surgically resected human stomach. Whole tissue lysates (60 μg) were loaded on 12% SDS–PAGE gels. Pairs of positive bands (the pair being due to the presence of splice variants) are observed in the antral (lane 1) and body mucosa (lane 2) at the same molecular weight (37 kDa) as observed in embryonic mouse brain.[14,16] The tissue sample from the fundic mucosa (lane 3) yields a faint band, but no pair. A pair of positive bands in the body mucosa may be due to the detection of pyloric glands extended from the antral area to the body area.

cells (Figure 1E). A similar pattern was obtained on double-staining for Msi-1 and Ki67, although there were fewer Ki67+ cells than PCNA+ cells (Figure 1F).

WESTERN BLOT ANALYSIS

The presence of Msi-1 expression in the adult human stomach was confirmed by Western blot analysis. On Western blot analysis using the Msi-1 antibody, a pair of positive bands (37 kDa) was observed in embryonic mouse brain, due to the presence of splice variants.[14,16] Similarly, in the present study, a pair of positive bands was observed in the antral mucosa of the human stomach at the same molecular weight as in embryonic mouse brain (Figure 2),[14,16] confirming the presence of Msi-1 protein in the human antrum. In contrast, the tissue sample from the fundic mucosa yielded a faint band, but not a pair, indicating absence of Msi-1 protein in the fundic mucosa.

Msi-1 EXPRESSION DURING DEVELOPMENT OF THE HUMAN STOMACH

By the 14th to the 17th weeks of gestation, gastric pits, neck regions, early glands and surface epithelial cells are present in most parts of the stomach. In the present study, Msi-1 expression during the 14th week was found to be concentrated in the epithelial cells in the basal regions of the pyloric glands (Figure 3A). By the 19th week, Msi-1+ cytoplasm was seen predominantly in the epithelial cells in the basal regions of the pyloric glands, although cells with PCNA+ nuclei were scattered throughout the entire epithelial cell population (Figure 3B). By the 20th to the 27th weeks, the number of Msi-1+ cells had increased; these cells were located predominantly in the lower to middle portions of the gastric glands of the antrum (Figure 3C). By the 22nd week, the PCNA+ cells had mostly moved to a higher position than the Msi-1+ cells, and the PCNA+ cells were concentrated in the epithelial cells in the pit regions of the glands (Figure 3C). The Msi-1+ cells showed no PCNA expression, as similarly seen in the gastric glands of adult human antrum (see the first section of Results).

PARTIAL COLOCALIZATION OF Msi-1 AND GASTRIC-TYPE MUCINS IN THE ADULT HUMAN ANTRUM

MUC5AC was strongly expressed by the surface epithelial and neck cells of both the gastric body and the antrum. On the other hand, MUC6 was expressed mainly in the pyloric gland cells of the antrum, following similar patterns to those described previously.[23] Double-staining for MUC6 and Msi-1 revealed that the distributions of the two antigens overlapped partly, and that Msi-1 expression was generally limited to the upper regions of MUC6+ glands (Figure 4A). Double-staining for MUC5AC and Msi-1 again demonstrated that the distributions of the two antigens overlapped partly and that Msi-1 expression was generally limited to the lower regions of the MUC5AC+ glands (Figure 4B). TFF1 expression, which is generally observed in the foveolar pit area, was less extensive than MUC5AC expression and coexpression of TFF1 and Msi-1 was not usually detected (Figure 4C).

DECREASED EXPRESSION OF Msi-1 IN IM

In the gastric glands showing IM, Msi-1 expression became weaker than in the gastric glands without IM (Figure 5A). Msi-1 expression was detectable predominantly in the cytoplasm of goblet and columnar cells, but was occasionally found in the nucleus. In the gastric glands showing incomplete IM, Msi-1 expression was detected in 15 out of the 31 specimens (48.4%); however, > 50% positivity was found in only one specimen (Table 1). In the gastric glands showing complete IM (Figure 5B), no Msi-1 reactivity was detected in 24 out of the 31 tissue samples (77.4%), and > 50% positivity was not found in any specimen (Table 1). The percentages of Msi-1 positivity in complete IM were lower than those in incomplete IM at all levels of Msi-1 reactivity (Table 1).

Discussion

As in the fetal rat stomach,[24,25] during the earliest stages of development of the human stomach, the proliferative regions (progenitor zones) are located in the basal regions of the glands. As development of the pit

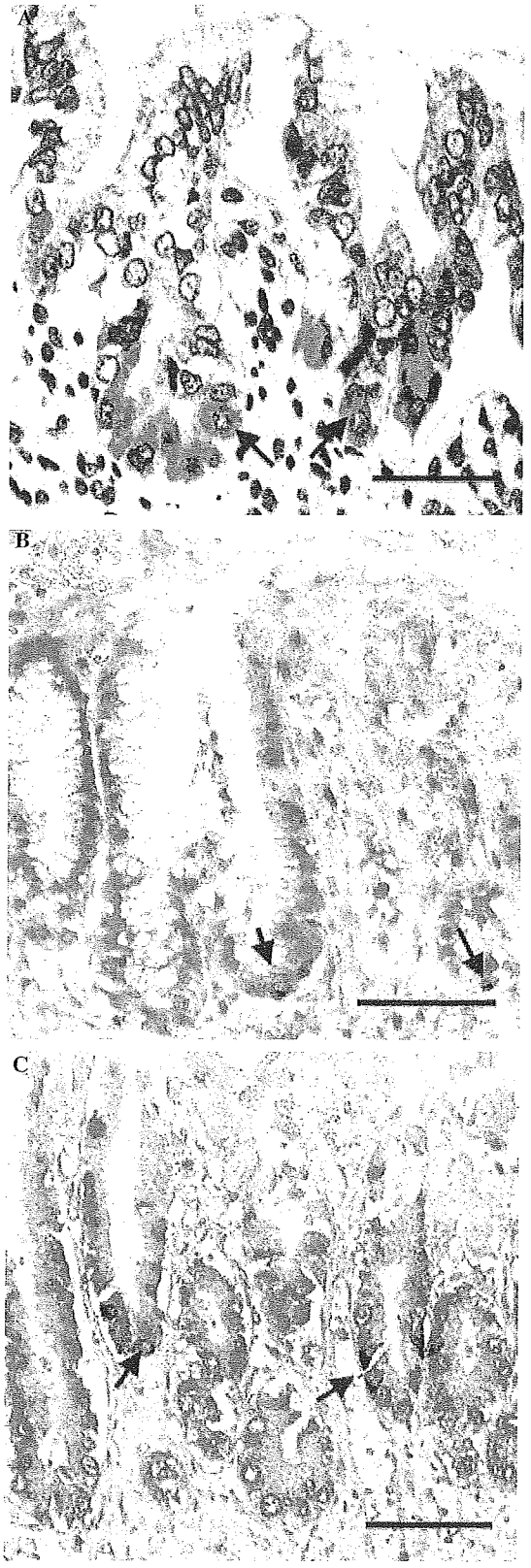

gland proceeds, the proliferative region moves upwards, and is limited to the isthmus/neck region in the adult human stomach.[24] The changing pattern of distribution of the proliferative regions is similar to that of the localization of Msi-1+ cells in the developing gastric glands. Msi-1 expression was present specifically in the basal regions of early glands and subsequently moved upwards, finally establishing an adult location in the isthmus/neck region, where adult putative progenitor cells are thought to be actively proliferating. Indeed, in the present study, double-staining for Msi-1 and PCNA demonstrated that Msi-1+ cells were located among the actively proliferating cells in the isthmus/neck region of the adult human antrum. These results indicate that the transient expression of Msi-1 coincides well with the actively proliferative regions containing progenitor cells in both fetal and adult gastric glands in the antrum. A similar trend in the expression pattern of Msi-1 has been reported in the mouse small intestine, where Msi-1 is expressed specifically within the small intestinal crypts, and putative stem cells and at least the next two generations are positive for Msi-1.[15] The positive correlation between the distribution of Msi-1+ cells and that of the proliferative regions in the gastric glands suggests that Msi-1+ cells have progenitor cell characteristics in the human antrum.[6]

A previous study has shown that Msi-1 expression correlates well with the proliferative activity of human brain tumours.[26] Similarly, Msi-1+ neural stem and progenitor cells induced by ischaemia in the rat hippocampus show bromodeoxyuridine expression.[20] These observations indicate that Msi-1 expression can correlate positively with proliferative activity in these

Figure 3. Msi-1 expression in the fetal human antrum. **A**, By the 14th week of gestation, the pit/gland structure has elongated, while the surface columnar epithelial cells have differentiated and exhibit cytoplasm with basal nuclei. Msi-1 expression (arrows) is concentrated in the basal regions of the pyloric glands. **B**, Double-staining for proliferating cell nuclear antigen (PCNA) and Msi-1 in the pyloric glands at the 19th week of gestation. Cells with Msi-1+ cytoplasm (brown labelling) are seen predominantly in the epithelial cells in the basal regions of the pyloric glands, although cells with PCNA+ nuclei (red labelling) are scattered throughout the entire epithelial cell population. The arrows indicate cells with an Msi-1+ cytoplasm. **C**, Double-staining for PCNA and Msi-1 in the gastric glands of the antrum at the 22nd week of gestation. Along with a concomitant increase in the heights of the pits and glands, the PCNA+ cells are concentrated in the epithelial cells in the pit regions of the glands. By the 22nd week of gestation, most cells with PCNA+ nuclei (red labelling) have moved to a higher position than cells with Msi-1+ cytoplasm (brown labelling). The arrows indicate cells with an Msi-1+ cytoplasm but devoid of nuclear PCNA staining. The double-staining was visualized using DAB (brown labelling) and fuchsin (red labelling) substrates. Bars are 20 μm (A), 40 μm (B), and 40 μm (C).

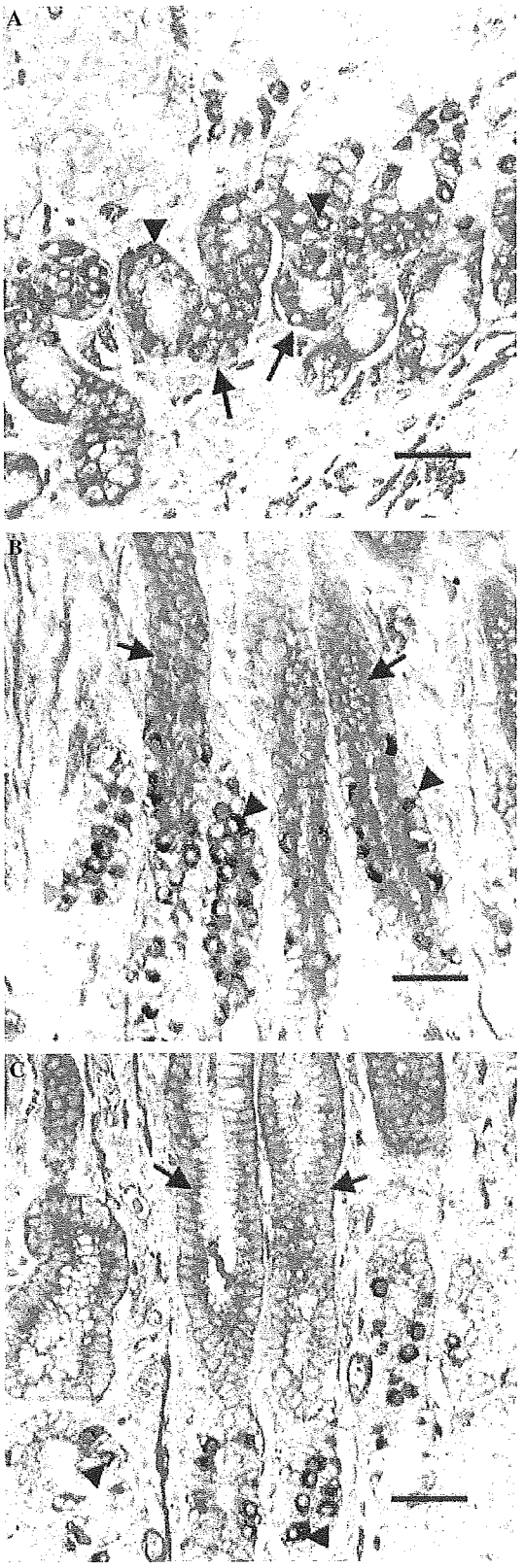

cell types.[26–28] Supportive evidence has been reported in the amphibian gastrointestinal tract during metamorphosis, in which Msi-1 and PCNA are coexpressed in the stomach.[6] However, in the present study the Msi-1+ cells in the proliferative regions showed no PCNA or Ki67 expression. A functional *in vitro* study of Msi-1 has shown that Notch signalling activity is increased by Msi-1 expression.[29] Activation of the Notch signalling pathway suppresses the differentiation of stem cells and plays a fundamental role in maintaining cells in an undifferentiated state. This suggests that the Msi-1+ cells within the proliferative regions of the human antrum may remain in an undifferentiated state and not express PCNA or Ki67.[30] Along with the partial differentiation of Msi-1+ cells, the Msi-1+ cells may begin to proliferate actively, which leads to the rapid down-regulation of Msi-1 expression together with the expression of PCNA or Ki67. Therefore, Msi-1 can be useful for identifying progenitor cells before active proliferation in the human antrum.

Specific antibodies against the various mucins are used to define gastric phenotypes. These include the MUC5AC antibody, which is specific for gastric foveolar-type mucin, and the MUC6 antibody, which is specific for pyloric gland-type mucin.[31] In the present study, the distribution of Msi-1 overlapped partly with that of MUC5AC and MUC6. Furthermore, Msi-1 expression was generally limited to the upper regions of the glands positive for MUC5AC and the lower regions of the glands positive for MUC6. Since epithelial cell differentiation and gastric gland migration are thought to be closely linked,[24,25] Msi-1+ cells located in the upper or lower glandular regions could move upwards or downwards, and then differentiate into foveolar or pyloric gland cells, respectively. This suggests that Msi-1+ cells retain at least some features

Figure 4. Partial colocalization of Msi-1 and gastric-type mucins in the adult human antrum. **A**, The arrows indicate MUC6+ cells (red labelling), which are almost all present among the epithelial cells in the pyloric glands. The black arrowheads indicate Msi-1+ cells (brown labelling), which are located mainly in the upper region of the MUC6+ glands. MUC6 expression gradually decreases toward the upper region of the glands, and Msi-1+ cells devoid of MUC6 expression (blue arrowheads) are visible. **B**, The arrows indicate MUC5AC+ cells (red labelling), which are almost all present throughout the foveolar cell population. The black arrowheads indicate Msi-1+ cells (brown labelling), which are located mainly in the lower regions of the MUC5AC+ glands. Msi-1+ cells devoid of MUC5AC expression (blue arrowheads) are also detected. **C**, There is no coexpression of TFF1 and Msi-1 in the gastric glands of the antrum. The arrows indicate TFF1+ cells (red labelling) and the arrowheads indicate Msi-1+ cells (brown labelling). The double-staining was visualized using DAB (brown labelling) and fuchsin (red labelling) substrates. All bars are 50 μm.

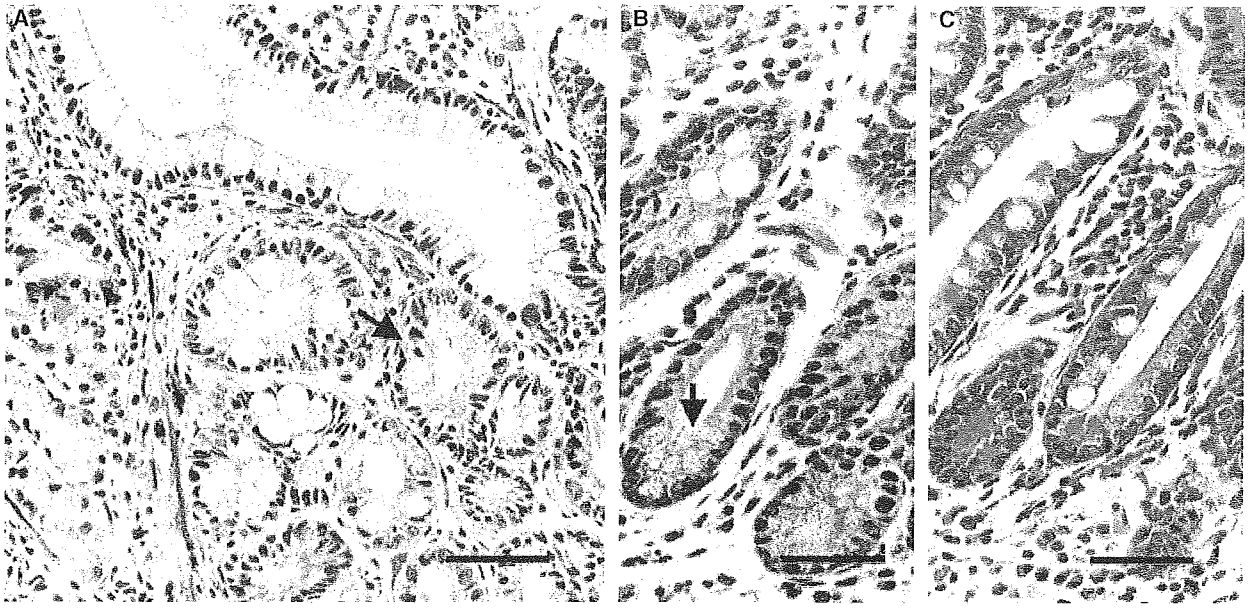

Figure 5. Decreased expression of Msi-1 in intestinal metaplasia (IM). A, Msi-1 expression in incomplete IM becomes weaker than that in the gastric glands without IM. The arrow indicates the Msi-1+ metaplastic epithelial cell and the blue arrowhead indicates the Msi-1+ epithelial cell in the gastric glands without IM. B, Weak Msi-1 expression is detected in the metaplastic epithelial cells of complete IM. The arrow indicates Msi-1 reactivity in the cytoplasm of the epithelial cell adjacent to Paneth cells. C, H&E-stained serial section from the metaplastic region of complete IM in B. All bars are 50 μm.

Table 1. Grading of reactive cells in each Msi-1 staining of intestinal metaplasia (IM) glands in human stomach

	Grading by percentage of reactive cells				
Type of IM	Grade 0 0	Grade 1 0 < x < 20%	Grade 2 20% < x < 50%	Grade 3 50% < x	Total number of tissue samples
Incomplete	16 (51.6%)	8 (25.8%)	6 (19.3%)	1 (3.2%)	31
Complete	24 (77.4%)	6 (19.3%)	1 (3.2%)	0	31

characteristic of both foveolar and pyloric gland cell differentiation phenotypes.

Another interesting finding of the present study is that Msi-1 expression is decreased in the IM cells of the human stomach. Several recent studies have indicated that Msi-1 appears to be preferentially expressed in the early generations of cell lineages in mouse small intestine and colon.[15,32] In the present study, however, Msi-1 expression was markedly decreased in IM cells of the human stomach. The difference in the patterns of Msi-1 expression between normal intestine and metaplasia supports the assumption that IM is a consequence of abnormal differentiation, in which, as has previously been proposed,[33] stem cells or progenitor cells may not differentiate into any of the normal intestinal epithelial phenotypes. At the present time, the mechanism governing Msi-1 protein expression in the adult human antrum is still unknown. Functional studies are needed to clarify the characteristics of Msi-1+ cells as progenitor cells and the role of Msi-1 protein in the regulation of normal epithelial cell differentiation and metaplastic change in the human antrum.

References

1. Kirkland SC. Clonal origin of columnar, mucous, and endocrine cell lineages in human colorectal epithelium. *Cancer* 1988; **61**; 1359–1363.
2. Ponder BA, Schmidt GH, Wilkinson MM *et al.* Derivation of mouse intestinal crypts from single progenitor cells. *Nature* 1985; **313**; 689–691.
3. Brittan M, Wright NA. Gastrointestinal stem cells. *J. Pathol.* 2002; **197**; 492–509.
4. Modlin IM, Kidd M, Lye KD, Wright NA. Gastric stem cells: an update. *Keio J. Med.* 2003; **52**; 134–137.
5. Brittan M, Wright NA. Stem cell in gastrointestinal structure and neoplastic development. *Gut* 2004; **53**; 899–910.

6. Ishizuya-Oka A, Shimizu K, Sakakibara S, Okano H, Ueda S. Thyroid hormone-upregulated expression of Musashi-1 is specific for progenitor cells of the adult epithelium during amphibian gastrointestinal remodeling. *J. Cell Sci.* 2003; **116**; 3157–3164.
7. Hattori T, Fujita S. Tritiated thymidine autoradiographic study of cell migration and renewal in the pyloric mucosa of golden hamsters. *Cell Tissue Res.* 1976; **175**; 49–57.
8. Karam SM, Leblond CP. Dynamics of epithelial cells in the corpus of the mouse stomach. I. Identification of proliferative cell types and pinpointing of the stem cell. *Anat. Rec.* 1993; **236**; 259–279.
9. Karam SM, Leblond CP. Dynamics of epithelial cells in the corpus of the mouse stomach. II. Outward migration of pit cells. *Anat. Rec.* 1993; **236**; 280–296.
10. Karam SM, Straiton T, Hassan WM, Leblond CP. Defining epithelial cell progenitors in the human oxyntic mucosa. *Stem Cells* 2003; **21**; 322–336.
11. Nakamura M, Okano H, Blendy JA, Montell C. Musashi, a neural RNA-binding protein required for Drosophila adult external sensory organ development. *Neuron* 1994; **13**; 67–81.
12. Sakakibara S, Imai T, Hamaguchi K *et al.* Mouse-Musashi-1, a neural RNA-binding protein highly enriched in the mammalian CNS stem cell. *Dev. Biol.* 1996; **176**; 230–242.
13. Good P, Yoda A, Sakakibara S *et al.* The human Musashi homolog 1 (MSI1) gene encoding the homologue of Musashi/Nrp-1, a neural RNA-binding protein putatively expressed in CNS stem cells and neural progenitor cells. *Genomics* 1998; **52**; 382–384.
14. Kaneko Y, Sakakibara S, Imai T *et al.* Musashi1: an evolutionally conserved marker for CNS progenitor cells including neural stem cells. *Dev. Neurosci.* 2000; **22**; 139–153.
15. Kayahara T, Sawada M, Takaishi S *et al.* Candidate markers for stem and early progenitor cells, Musashi-1 and Hes1, are expressed in crypt base columnar cells of mouse small intestine. *FEBS Lett.* 2003; **535**; 131–135.
16. Potten CS, Booth C, Tudor GL *et al.* Identification of a putative intestinal stem cell and early lineage marker; musashi-1. *Differentiation* 2003; **71**; 28–41.
17. Kawachi T, Kogure K, Tanaka N, Tokunaga A, Sugimura T. Studies of intestinal metaplasia in the gastric mucosa by detection of disaccharidases with 'Tes-Tape'. *J. Natl Cancer Inst.* 1974; **53**; 19–30.
18. Kanemura Y, Sakakibara S, Okano H. Identification of Musashi1-positive cells in human normal and neoplastic neuroepithelial tissues by immunohistochemical methods. *Meth. Mol. Biol.* 2002; **198**; 273–281.
19. Waiser J, Schwaar S, Bohler T *et al.* Immunohistochemical double-staining of renal allograft tissue: critical assessment of three different protocols. *Virchows Arch.* 2002; **440**; 648–654.
20. Yagita Y, Kitagawa K, Ohtsuki T *et al.* Neurogenesis by progenitor cells in the ischemic adult rat hippocampus. *Stroke* 2001; **32**; 1890–1896.
21. Liu Y, Tolbert EM, Lin L *et al.* Up-regulation of hepatocyte growth factor receptor: an amplification and targeting mechanism for hepatocyte growth factor action in acute renal failure. *Kidney Int.* 1999; **55**; 442–453.
22. Yang J, Dai C, Liu Y. Hepatocyte growth factor gene therapy and angiotensin II blockade synergistically attenuate renal interstitial fibrosis in mice. *J. Am. Soc. Nephrol.* 2002; **13**; 2464–2477.
23. Reis CA, David L, Correa P *et al.* Intestinal metaplasia of human stomach displays distinct patterns of mucin (MUC1, MUC2, MUC5AC, and MUC6) expression. *Cancer Res.* 1999; **59**; 1003–1007.
24. Menard D, Arsenault P. Cell proliferation in developing human stomach. *Anat. Embryol.* 1990; **182**; 509–516.
25. Yang DH, Tsuyama S, Ge YB *et al.* Proliferation and migration kinetics of stem cells in the rat fundic gland. *Histol. Histopathol.* 1997; **12**; 719–727.
26. Okano H, Imai T, Okabe M. Musashi: a translational regulator of cell fate. *J. Cell Sci.* 2002; **115**; 1355–1359.
27. Kanemura Y, Mori K, Sakakibara S *et al.* Musashi1, an evolutionarily conserved neural RNA-binding protein, is a versatile marker of human glioma cells in determining their cellular origin, malignancy, and proliferative activity. *Differentiation* 2001; **68**; 141–152.
28. Toda M, Iizuka Y, Yu W *et al.* Expression of the neural RNA-binding protein Musashi1 in human gliomas. *Glia* 2001; **34**; 1–7.
29. Imai T, Tokunaga A, Yoshida T *et al.* The neural RNA-binding protein Musashi1 translationally regulates mammalian numb gene expression by interacting with its mRNA. *Mol. Cell Biol.* 2001; **21**; 3888–3900.
30. Sakakibara S, Nakamura Y, Yoshida T *et al.* RNA-binding protein Musashi family: roles for CNS stem cells and a subpopulation of ependymal cells revealed by targeted disruption and antisense ablation. *Proc. Natl Acad. Sci. USA* 2002; **99**; 15194–15199.
31. Shiroshita H, Watanabe H, Ajioka Y *et al.* Re-evaluation of mucin phenotypes of gastric minute well-differentiated-type adenocarcinomas using a series of HGM, MUC5AC, MUC6, M-GGMC, MUC2 and CD10 stains. *Pathol. Int.* 2004; **54**; 311–321.
32. Nishimura S, Wakabayashi N, Toyoda K, Kashima K, Mitsufuji S. Expression of Musashi-1 in human normal colon crypt cells: a possible stem cell marker of human colon epithelium. *Dig. Dis. Sci.* 2003; **48**; 1523–1529.
33. Tatematsu M, Tsukamoto T, Inada K. Stem cells and gastric cancer: role of gastric and intestinal mixed intestinal metaplasia. *Cancer Sci.* 2003; **94**; 135–141.

The RNA-binding protein HuD regulates neuronal cell identity and maturation

Wado Akamatsu*†, Hiroaki Fujihara‡, Takayuki Mitsuhashi§, Masato Yano*, Shinsuke Shibata*, Yoshika Hayakawa*¶, Hirotaka James Okano*, Shin-ichi Sakakibara‖, Hiroshi Takano**, Toshiya Takano‡, Takao Takahashi§, Tetsuo Noda**, and Hideyuki Okano*††‡‡

Departments of *Physiology, ‡Microbiology, and §Pediatrics, Keio University School of Medicine, Tokyo 160-8582, Japan; ‖Department of Histology and Neurobiology, Dokkyo University School of Medicine, Tochigi 321-0293, Japan; **Department of Molecular Genetics, Tohoku University School of Medicine, Sendai 980-8575, Japan; and ††Core Research for Evolutional Science and Technology, Japan Science and Technology Agency, Saitama 332-0012, Japan

Edited by Yuh Nung Jan, University of California School of Medicine, San Francisco, CA, and approved February 4, 2005 (received for review October 11, 2004)

Neural Hu proteins (HuB/C/D) are RNA-binding proteins that have been shown to induce neuronal differentiation activity when overexpressed in immature neural progenitor cells or undifferentiated neuronal tumors. Newly generated *HuD*-deficient mice exhibited a transient impaired-cranial-nerve-development phenotype at an early embryonic stage. Adult *HuD*-deficient mice exhibited an abnormal hind-limb reflex and poor rotarod performance. Analysis of neurosphere formation revealed that the number and self-renewal capacity of the neural stem/progenitor cells were increased in *HuD*-deficient mice. *HuD*-deficient primary neurospheres also generated a smaller number of neurons. Cohort analysis of the cellular proliferative activity by using BrdUrd and iododeoxuridine labeling revealed that the number of differentiating quiescent cells in the embryonic cerebral wall was decreased. Long-term administration of BrdUrd revealed that the number of slowly dividing stem cells in the adult subventricular zone was increased in the *HuD*-deficient mice. Taken together, the results suggest that HuD is required at multiple points during neuronal development, including negative regulation of proliferative activity and neuronal cell-fate acquisition of neural stem/progenitor cells.

ELAV | Hu | neural stem cell

Hu proteins have been identified as the target antigens of autoantibodies appearing in the sera of patients with paraneoplastic encephalomyelitis (1). By molecular cloning, four members of the Hu protein family have been identified as RNA-binding proteins that resemble the *Drosophila* ELAV protein (1–4). These mammalian Hu/ELAV proteins, with the exception of HuA (HuR), are widely expressed in both early postmitotic and mature neurons; HuA (HuR), however, is expressed ubiquitously. All members of the Hu family proteins contain three RNA-recognition motifs, and their structures are highly conserved. Previous reports have suggested the binding of Hu proteins to several putative target mRNAs, both *in vitro* and *in vivo*. Because most of the target mRNAs have AU-rich elements in their untranslated regions, Hu proteins possibly regulate the stability or translational efficiency of their target mRNAs. Most of these putative target genes are involved in cellular proliferation [p21 (5), p27 (6), c-fos, and N-Myc (7)] or are important in the formation of neurites [Neurofilament-M (8), GAP-43 (9), and tau (10, 11)].

Thus, Hu proteins have been considered to be involved in the differentiation and/or maintenance of neurons. Previously, we reported, by a gene transfer experiment conducted with the electroporation method, that overexpression of HuB/HuC induces neuronal differentiation in PC12 cells and in the periventricular immature neural stem or progenitor cells of embryonic mice (12). HuD has also been shown to have similar functions in PC12 cells (13). It has been also reported that antisense-mediated knockdown of HuC results in impaired spatial learning performance in mice, with concomitant down-regulation of GAP-43 expression (14). These findings indicate the possible involvement of the Hu proteins in the sprouting and regeneration of neurons. In this paper, we report on the phenotype of mice with targeted disruption of the *HuD* gene, whose expression commences even earlier than that of HuC, another member of the same family (4), and continues to be seen even in mature neurons.

Materials and Methods

Generation of *HuD*-Deficient mice. *HuD*-deficient mice were generated by a method similar to one described previously (15). Briefly, a 2.5-kb fragment containing intronic sequences upstream and a 6.1-kb fragment containing intronic sequences downstream of the second exon that contains the second RNA-recognition motifs (25–265 bp of cDNA) were inserted into the target plasmid vector to delete a 1.0-kb genomic DNA fragment and induce a frame shift. RT-PCR analysis was performed by using the primers 5′-AGAAGGGAATGTCAGCTTTT-3′ (exon 1) and 5′-TGAATTCCTCTTGGGTCATA-3′ (exon 2), or 5′-TATGACCCAAGAGGAATTCA-3′ (exon 2) and 5′-TGGTCTTGGGAAGGCCACTA-3′ (exon 3).

Immunoblotting was performed with the same method as described (12). Anti-HuD monoclonal antibody 16C12 (Clonegene, Hartford, CT) was used in 1:500 dilutions. Anti-HuB/C/D human serum (a gift from Robert Darnell, The Rockefeller University, New York) was used in 1:2,000 dilutions.

Whole-Mount Immunohistochemistry. Whole-mount immunohistochemistry of the embryonic mice was performed as described (16).

Analysis of Motor Functions. Mice of each genotype that were 20–26 weeks old were used for the analysis. Each mouse was placed on a 3.5-cm-diameter rod covered with rubber to evaluate its rotarod performance: The mice were left on the rod for 1 min for habituation. The rotarod was then rotated at 20 rpm, and the performance of the mice was measured in terms of latency (time successfully spent on the rotating rod without falling off). Six trials were conducted for each individual. Mice that stayed on the rotarod for 300 s were considered complete responders, and their latencies were recorded as 300 s.

Cell Culture and Immunocytochemistry. Cells from the ganglionic eminence or cerebral cortex of embryonic day (E)14.5 embryos

This paper was submitted directly (Track II) to the PNAS office.

Abbreviations: IdUrd, iododeoxuridine; SVZ, subventricular zone; E*n*, embryonic day *n*; P, proliferative; Q, quiescent.

†To whom correspondence may be sent at the present address: Department of Medical Genetics and Microbiology, University of Toronto,1 King's College Circle, Toronto, ON, Canada M5S 1A8. E-mail: wado.akamatsu@utoronto.ca.

¶Present address: Department of Neurobiology, Graduate School of Medicine, Gifu University, Gifu 501-1194, Japan.

‡‡To whom correspondence should be addressed. E-mail: hidokano@sc.itc.keio.ac.jp.

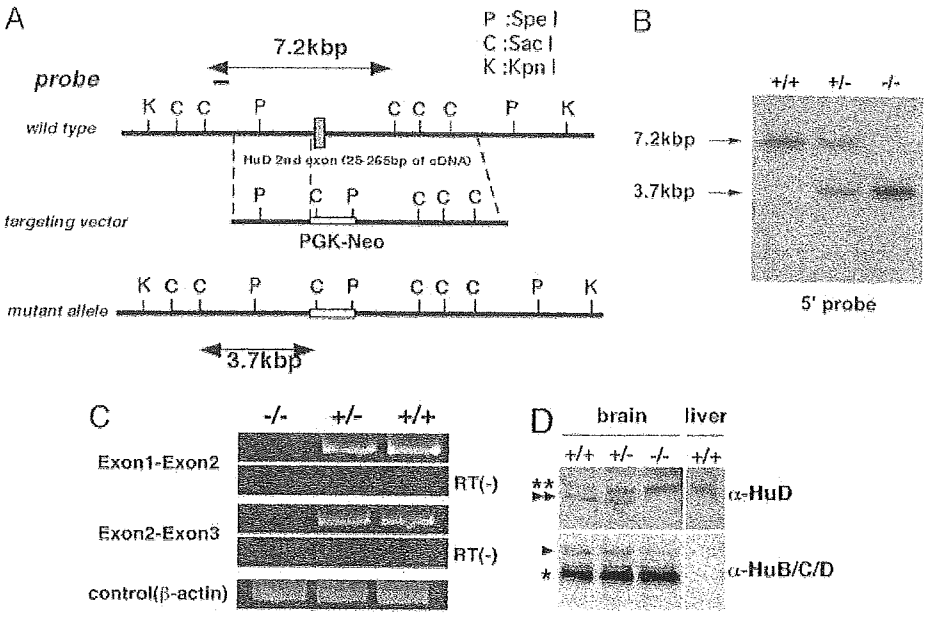

Fig. 1. Targeting strategy, germ-line transmission, and expression analysis of the *HuD* gene. (*A*) Organization of the target vector, the mouse *HuD* gene, and the allele resulting from homologous recombination. An exon (black box) of the *HuD* allele containing the initiation codon was replaced with a PGK-neocassette. A 0.7-kb *Bam*HI-*Eco*RI fragment (5′ probe) was used to screen for recombinant alleles, and the sizes of the recombinant and wild-type fragments after *Sac*I digestion are shown (bidirectional arrows). (*B*) Germ-line transmission was confirmed by Southern blot analysis of *Sac*I-digested tail DNA from a litter of F_1 mice, using a 5′ probe. (*C*) The deletion of the *HuD* mRNA from the adult brains of homozygous animals was confirmed by RT-PCR analysis. No amplified bands were observed from the RT samples of the *HuD* −/− brains, using either of the primer pairs (Exon 1-Exon 2 and Exon 2-Exon 3). (*D*) Immunoblots of adult brain or liver lysates with anti-HuD 16C12 monoclonal antibody (*Upper*) or anti-HuB/C/D serum (*Lower*). The bands indicated by a double arrowhead represent the HuD protein (*Upper*) and are missing in the liver lysates from the wild-type mice. The bands indicated by the double asterisk (*Upper Left*) represent nonspecific background immunoreactivity, which was also observed in negative control using wild-type liver lysates (*Upper Right*).

were cultured as described (17). For the differentiation assays of the neurospheres, neurospheres were plated as described (15). Subsequently, triple-label immunostaining was performed to examine their differentiation into neurons, astroglia, and oligodendroglia, as described (18).

Cohort Analysis of Cellular Proliferation in the Embryonic Cerebral Wall. This experimental concept was identical to one described previously (19), except that iododeoxuridine (IdUrd) was used in place of tritiated thymidine. (Also see Fig. 6, which is published as supporting information on the PNAS web site.) Proliferating cells of the embryonic cerebral wall were exposed sequentially, by i.p. injection, to the S phase marker IdUrd (50 mg/g of body weight; Sigma) and BrdUrd (50 mg/g of body weight; Sigma). Briefly, IdUrd was injected at 8:00 a.m. in both (P + Q and Q) protocols. Then BrdUrd was injected at 10:00 a.m., 1:00 p.m., 4:00 p.m., and 7:00 p.m. in the protocol for Q. In the protocol for P + Q, BrdUrd was injected only at 10:00 a.m. Animals in both protocols were killed and fixed at 10:30 p.m. (14.5 h from initial IdUrd injection). These protocols yielded separate values for the number of Q cells [N(Q)] and P + Q cells [N(P + Q] in 2 h (8:00–10:00 a.m.) cohort (19) (for details, see Fig. 6 legend). Immunohistochemical staining was performed on 4-μm paraffin-embedded coronal sections. Anti-BrdUrd labeling was performed as described (19). Anti-IdUrd staining was performed by using the anti-IdUrd monoclonal antibody, IU4 (Caltag, South San Francisco), which reacts with both BrdUrd and IdUrd. For visualization of the IdUrd-positive cells, Vectastain-AP and the alkaline phosphatase substrate kit (Vector Laboratories) were used. Blue cells without horseradish peroxidase signals represented the cells showing positive labeling for IdUrd but not for BrdUrd (Q cells).

Detection of Apoptosis. Evaluation of apoptosis was performed in E14.5 4-μm paraffin-embedded sections by using Apoptag (Intergen, Purchase, NY).

Long-Term BrdUrd Labeling of Slowly Dividing Cells. BrdUrd (1 mg/ml) was given, mixed with drinking water, to 20- to 24-week-old adult *HuD*−/− mice and their littermates for 4 weeks, followed by a 1-week BrdUrd free-chase period to wash out rapidly dividing cells. Four-micrometer-thick paraffin-embedded sections were immunostained as described for the embryonic sections. The number of BrdUrd-positive cells was counted in one-half of five independent sections for each frontal level.

Statistical Analysis. The statistical significance of differences was analyzed by using Student's *t* test ($n > 3$, each group). All values were expressed as mean ± SEM. Asterisks on the error bars denote statistical significance ($P < 0.05$).

Results

Targeted Disruption of the *HuD* Gene. Targeted disruption of the *HuD* locus in ES cells was performed and confirmed as described in Fig. 1 *A* and *B*. Interbreeding of the heterozygous mutant (*HuD*+/−) mice yielded homozygous mutant (*HuD*−/−) pups with the expected Mendelian ratio, indicating that HuD may not be essential for embryonic viability. We confirmed the absence of *HuD* mRNA (Fig. 1*C*) in adult homozygous mouse brains by RT-PCR. To demonstrate the absence of the HuD protein in *HuD*−/− mice, we performed immunoblotting of brain lysates with anti-HuD-specific monoclonal antibody 16C12 (Fig. 1*D Upper Left*) and anti-HuB/C/D serum (Fig. 1*D Lower Left*). Liver lysates of wild-type mice were also characterized with these antibodies as negative controls (see Fig. 1*D* legend). In *HuD*−/− mice, the band corresponding to HuD (indicated by the double arrowhead, Fig. 1*D Upper Left*) was absent in the immunoblot with the anti-HuD antibody. The results of the immunoblot with anti-HuB/C/D serum are shown in Fig. 1*D Lower*. The level of expression of the band indicated by the single asterisk was not significantly changed in the *HuD*−/− brain, whereas the expression of the band indicated by the single arrowhead decreased. Taken together, these results show that expression of HuD protein is missing, and expression of HuB/C proteins is unlikely to be strongly affected in *HuD*−/− mice, although we cannot exclude the possibility of attenuated expression of other splice variants of HuB/HuC by this immunoblot.

Neural Development and Motor Functions in *HuD*-Deficient Mice. We first visualized and evaluated the midembryonic nervous system development of *HuD*−/− animals by using whole-mount immu-

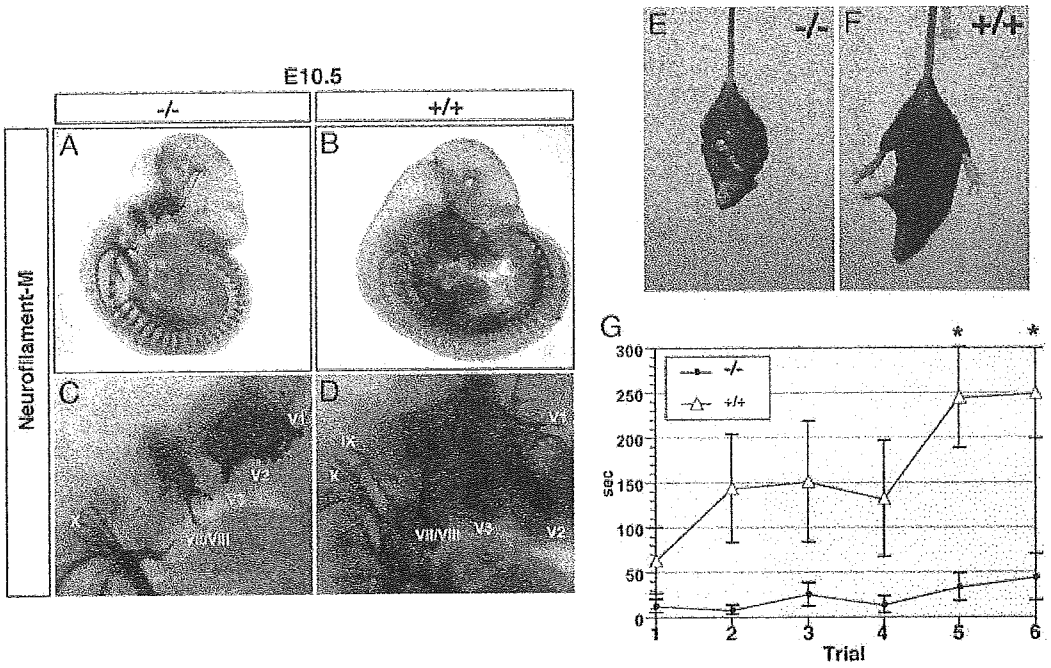

Fig. 2. Histological analysis of the *HuD*-deficient mouse embryos. (*A–D*) Lateral views of E10.5 embryos of *HuD*−/− mice (*A* and *C*) and their wild-type littermates (*B* and *D*) stained with 2H3 antineurofilament-M antibody. In the wild-type embryos, axons of the glossopharyngeal nerve (IX) and hypoglossal nerve (XII) are seen extending from the caudal hindbrain and rostral spinal cord. On the other hand, the axons of these cranial nerves are not visualized in the *HuD*−/− embryos. Development of other cranial nerves, including the trigeminal (V) and acousticofacial (VII/VIII) nerves, also seems to be impaired in the *HuD*-deficient embryos as compared with that in their wild-type littermates. (*E* and *F*) The hind-feet-clenching phenotype in adult *HuD*−/− mice at 24 weeks of age. The *HuD*−/− mice displayed hind-feet-clenching behavior when picked up by the tail from 4 to 8 weeks of age (*E*). In wild-type littermates, however, the angles of the hind feet were close to a right angle (*F*). (*G*) Rotarod analysis. *HuD*−/− and their wild-type littermates at 20–26 weeks of age were used for the analysis. In *HuD*−/− mice, improvement of retention time by learning could scarcely be seen. The retention time was significantly shorter in the *HuD*−/− mice than in the wild-type littermates in the fifth and sixth trials.

nostaining of Neurofilament-M at the stage of E10.5, when HuD-positive mature neurons normally extend neurites toward the ventral neural tube (Fig. 2 *A–D*). We observed that the neurite extension of several cranial nerves [glossopharyngeal nerve (IX), hypoglossal nerve (XII), trigeminal nerve (V), and acousticofacial (VII/VIII) nerves] was impaired in most *HuD*−/− embryos (Fig. 2 *A* and *C*). However, no such developmental delay of the nervous system was observed in later-stage embryos. In E14 and E16 embryonic sections, the expression of neuroepithelial markers (Nestin or Musashi-1) in the VZ remained undisturbed (data not shown). No morphological abnormalities of the central nervous system were observed in E14 embryos (Fig. 7 *A* and *B*, which is published as supporting information on the PNAS web site), indicating that the above-mentioned impaired-cranial-nerve-development phenotype appeared only transiently. The apparent masking of the cranial-nerve-phenotype in the later-stage embryos could perhaps be explained by the sequential onset of expression of the other Hu proteins in the developing nervous system (4).

HuD−/− pups were indistinguishable from their wild-type littermates during the first several postnatal weeks, in terms of both their size and appearance. There were no significant differences between adult *HuD*−/− mice and their wild-type littermates with respect to the structure of the brain as evaluated by histological analysis. The structures of the cerebral cortex, cerebellum, and hippocampus were indistinguishable between *HuD*−/− mice and their wild-type littermates (Fig. 7 *C–F*). Although we could not find any significant morphological abnormalities between the two groups of mice in the adult spinal cord either, including the dorsal root ganglia (data not shown), by 4–8 weeks postnatally, 70–80% of the *HuD*−/− animals showed a consistently abnormal clasping reflex of the hind limbs upon being suspended by the tail, whereas age-matched wild-type animals extended their limbs normally (Fig. 2 *E* and *F*). This clasping phenotype is seen in mutant mice with cortical (20) and basal ganglia defects (21) and indicates the presence of motor/sensory defects in adult *HuD*-deficient mice. To determine whether *HuD* deficiency affected the sensory and/or motor functions of the mature nervous system, we conducted rotarod analysis to evaluate motor coordination in *HuD*−/− adults. (Fig. 2*G*). Six trials were performed for each individual, and the duration for which the mice could stay on an accelerating rotarod without falling was measured. It was found that the duration for which *HuD*−/− mice could stay on the rotarod without falling was significantly shorter than that of their wild-type littermates. When the test was repeated, although the performance of wild-type mice improved significantly after a few trials, *HuD*−/− mice continued to perform very poorly even after several trials. In addition, the reproductive performance of the *HuD*−/− mice was noted to be poor as compared with that of their wild-type littermates.

Analysis of the Neuronal Cell Lineage in *HuD*−/− Embryos. We then examined the role of HuD in neuronal cell lineage development by using the neurosphere assay, which is a selective culture system for neural stem/progenitor cells (18). The ganglionic eminence or cerebral cortex from E14.5 *HuD*−/− embryos, as well as their littermates as controls, was dissociated into single cells and cultured in the presence of EGF and FGF type 2 to generate neurospheres. The number of neurospheres formed under this condition is believed to reflect the number of spheres forming multipotent neural stem cells within the dissociated cell population. As shown in Fig. 3*A*, the number of primary neurospheres formed from the *HuD*−/− embryonic ganglionic eminence was 1.5-fold higher in

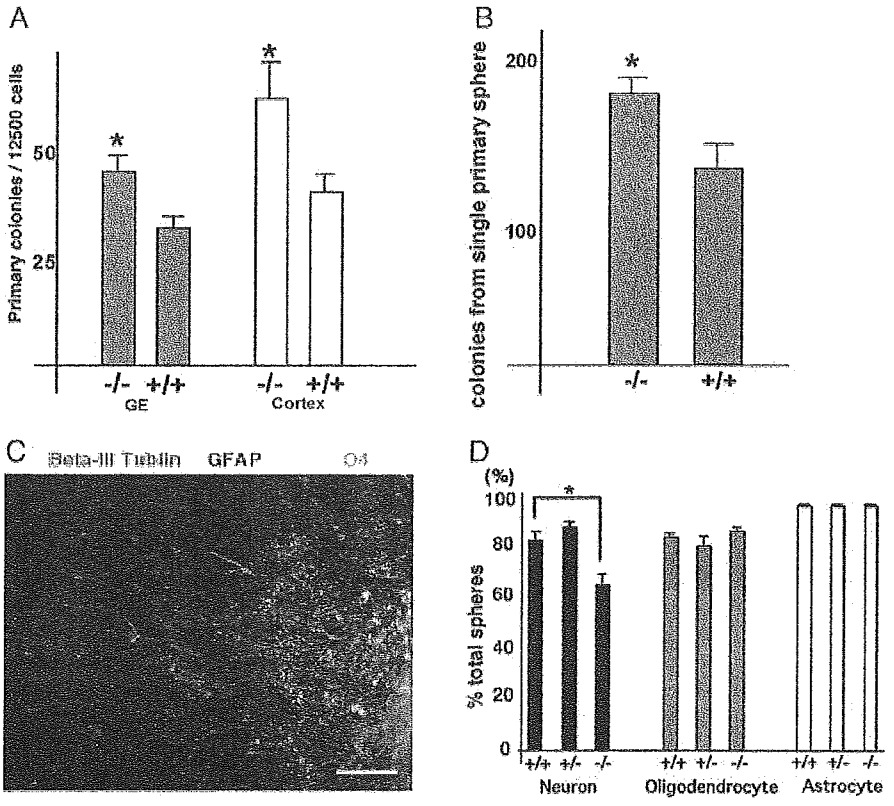

Fig. 3. Examination of neurosphere formation and differentiation in *HuD*-deficient embryos. (*A*) The number of neurospheres generated from 12,500 cells derived from the ganglionic eminence (GE) and cerebral cortex (Cortex) of E14.5 embryos, in 500 μl of the proliferation medium. (*B*) The number of secondary spheres derived from a single dissociated primary neurosphere is shown. (*C*) After allowing 72 h of differentiation of the primary neurospheres, the cell sheets generated from the neurospheres were fixed and triple-immunostained by using anti-TuJ1 (red), GFAP (blue), and O4 (green) antibodies. (Bar, 300 μm.) (*D*) The differentiation capacity of each primary neurosphere was determined based on the cell types contained in each clone. The clone types were analyzed for 100 spheres from each genotype.

HuD−/− mice than in their wild-type littermates. The number of primary spheres forming cells was also increased in the *HuD*−/− embryonic cerebral cortex. The number of secondary neurospheres generated from the subcloning of a single primary neurosphere may be considered as an estimate of the extent to which the initial primary neurosphere-forming stem cell undergoes symmetric divisions (18). The number of secondary neurosphere colonies was also significantly increased in E14.5 *HuD*−/− brains as compared with that in the brains of their wild-type controls (Fig. 3*B*), suggesting that the sphere-forming cells derived from E14.5 *HuD*−/− brains exhibited enhanced self-renewal capacity.

Next, we tested the multipotency of the neural stem cells by the differentiation assay; each neurosphere can be induced to differentiate into TuJ1-expressing neurons (N), GFAP-expressing astrocytes (A), and/or O4-expressing oligodendrocytes (O). After allowing differentiation to take place for 72 h, the cell sheets generated from the neurospheres were fixed and triple-immunostained by using anti-TuJ1, anti-GFAP, and anti-O4 antibody (Fig. 3*C*). Then, each sphere was analyzed for NAO expression. The number of spheres that generated neurons was significantly decreased to 0.8-fold in the *HuD*−/− embryos (Fig. 3*D*), whereas the number of spheres that generated oligodendrocytes and astrocytes remained unchanged (Fig. 3*D*). These observations indicate that the neural stem cells in E14.5 *HuD*−/− embryos have increased self-renewal ability and reduced ability to differentiate into neuronal progeny.

To investigate the *in vivo* kinetics of neurogenesis (production of postmitotic neurons) in the *HuD*-deficient embryonic cerebral wall, we performed sequential labeling for S phase markers by using IdUrd and BrdUrd, as described in previous reports, except that IdUrd was used in the place of tritiated thymidine (19). Using BrdUrd-only cumulative labeling, we could not observe any visible differences in the cell cycle length of the proliferative cells in the embryonic pseudostratified ventricular epithelium (PVE) between *HuD*−/− and wild-type mice (data not shown). Therefore, we concluded that 14.5 h of continuous BrdUrd exposure as described (22) was sufficiently long to cover the duration of the total cell cycle length (Tc); the S-phase length was then subtracted from Tc to calculate the percentage of mitotically Q cells, which represents the percentage of postmitotic neurons in this region. The distribution of Q cells and P + Q cells in the *HuD*−/− and wild-type embryos is shown in Fig. 4 *A* and *B*. In the case of the wild-type mice, the Q cells were mainly localized at a distance of 80–100 μm from the lateral ventricular surface, which corresponds to the position at which the cells leave the cell cycle and migrate out from the PVE (19). In the *HuD*−/− embryos, the number of Q cells (Fig. 4*B*) in these regions was decreased as compared with that in the wild-type embryos. In contrast, the number of P + Q cells (Fig. 4*A*) was not changed. Total numbers of P and P + Q cells in intermediate zone (bin6–16) are shown in Fig. 4*C*. The ratio of Q cells is calculated as N(Q)/N(P + Q). This value (Q fraction) represents the ratio of cells exit from cell cycles during G_1 phase. A decreased Q fraction in *HuD*−/− embryos suggests that the number and ratio of cells leaving the cell cycle are decreased, and that the P population in the developing cerebral wall is increased in the *HuD*−/− embryos and further suggests that in the absence of *HuD*, some of the neural stem/progenitor cells or committed neuronal progenitor cells fail to leave the cell cycle, resulting in reduced production of postmitotic neurons.

Macrocephaly has been described in several mutant mice lacking negative regulators of the cell cycle: Mice deficient in PTEN, a negative regulator of the cell cycle in neural stem cells (23), as well as those deficient in the cyclin-dependent kinase inhibitor p27(Kip1), a putative target of the Hu proteins (6, 24), show the macrocephaly phenotype in common, and these phenotypes are compatible with that predicted by theoretical simulation in the mathematical model of neocortical histogenesis (22). However, we found that the actual size of the postnatal brain was not larger in the

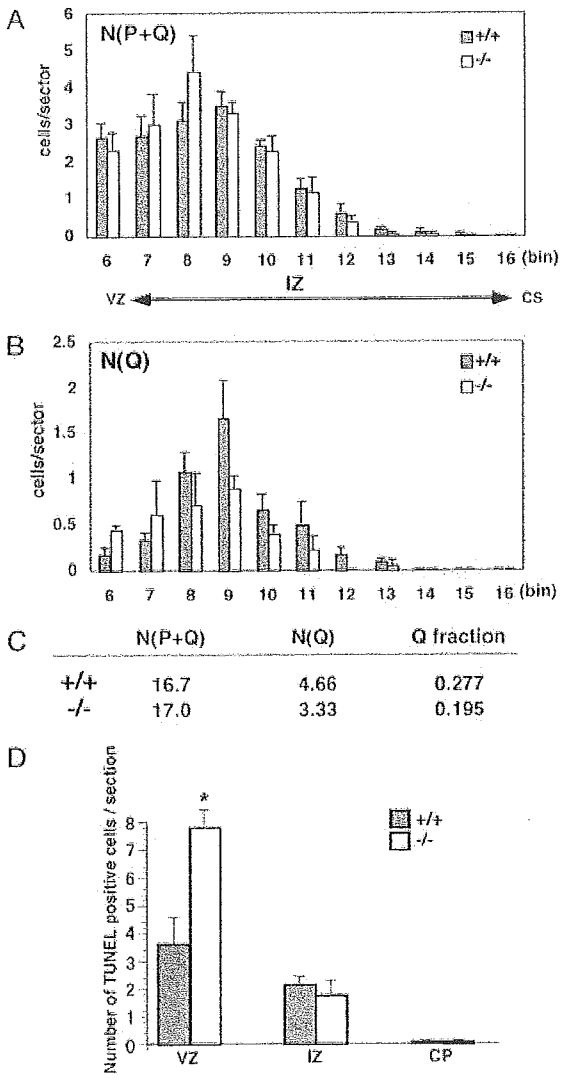

Fig. 4. Cohort analysis of cellular proliferation in the embryonic cerebral wall. (*A* and *B*) The distributions of the cells in the P + Q (*A*) or Q (*B*) fractions of the E14 *HuD*−/− and wild-type embryos. The analysis was undertaken in a coronal sector of the dorsomedial cerebral wall, ≈100 μm thick in its medial–lateral dimension and 4 μm thick (corresponding to the section thickness) in its rostral–caudal dimension. The sector was divided in its radial dimension into bins (*x* axis) 10 μm in height and numbered 1, 2, 3, and so on, from the ventricular margin. The numbers of cells in the Q or P + Q fraction [N(Q) or N(P+Q)] for each bin (*y* axis) were determined by counting only cells labeled by IdUrd in each protocol. IZ, intermediate zone; VZ, ventricular zone; and CS, cortical surface. (*C*) Total number of N(P + Q) and N(Q) cells in 5–16 bins is shown. Q fraction is calculated as N(Q)/N(P + Q). (*D*) Apoptotic cells in 4-μm-thick paraffin-embedded coronal sections of *HuD*−/− and wild-type embryos were detected by using the TUNEL method. The number of TUNEL-positive cells present along the lateral ventricular wall in the medial cerebral wall was counted. The apoptotic cells were then classified according to their location, based on the histological structure of the sections (IZ, intermediate zone; and CP, cortical plate).

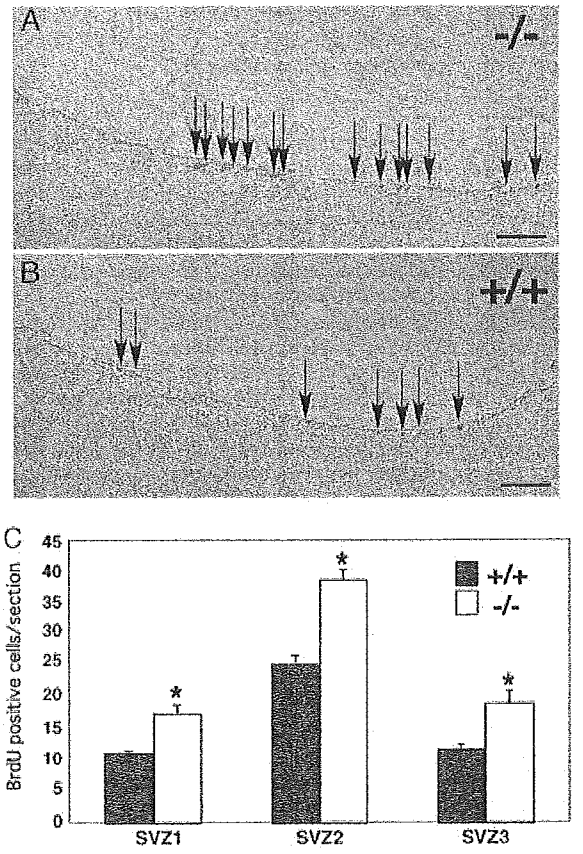

Fig. 5. Slowly dividing cells in the SVZ of adult *HuD*-deficient mice. (*A* and *B*) BrdUrd-labeled cells in the SVZ of *HuD*−/− mice (*B*) and their wild-type littermates were detected by immunostaining by using anti-BrdUrd monoclonal antibody. BrdUrd-positive cells are indicated by arrows. (Bar, 100 μm.) (*C*) The number of BrdUrd- positive cells in each of the frontal levels of the lateral SVZ in the animals was calculated. Three different frontal levels were analyzed. From rostral to caudal, slices were classified in three levels, SVZ1, SVZ2, and SVZ3 (also see Fig. 8).

HuD−/− mice. This discrepancy may be accounted for by increased apoptosis within the progenitor population. To investigate this possibility, we evaluated the status of apoptosis in the *HuD*−/− embryonic cerebral cortex (Fig. 4*D*). The number of apoptotic cells, as detected by the TUNEL method, was 2.2-fold higher in the ventricular zone, but not in the intermediate zone and cortical plate, of the *HuD*−/− as compared with that in their wild-type littermates. These data suggest that at least some of the cells that fail to leave the cell cycle undergo apoptosis, possibly due to their inability to undergo appropriate neuronal differentiation.

The Number of Slowly Dividing Stem Cells Is Increased in the SVZ of Adult *HuD*-Deficient Mice. It has been reported that several neurogenic regions are present in the adult mouse brain. Slowly dividing cells present in the adult SVZ are believed to exhibit neural stem-cell activities (25). To label slowly proliferating cells *in vivo*, adult *HuD*−/− and WT mice were administered BrdUrd continuously for 4 weeks, followed by a BrdUrd-free chase period of 1 week. For quantification of the labeled cells, we subdivided the lateral ventricle into three distinct coronal levels (Fig. 8, which is published as supporting information on the PNAS web site). Cells labeled with BrdUrd were visualized by immunohistochemical staining by using anti-BrdUrd antibody (Fig. 5 *A* and *B*). BrdUrd-positive cells were present within the SVZ along the lateral ventricular wall. At all of the coronal levels analyzed (SVZ1, -2, and -3), the total number of BrdUrd-positive cells was 1.5- to 2.0-fold higher in the *HuD*−/− mice than in their wild-type littermates (Fig. 5*C*).

These results taken together suggest that the neural stem/progenitor cells in both fetal (embryonic periventricular and embryonic ganglionic eminence cells; Figs. 3 and 4) and adult (SVZ cells in the adult; Fig. 5) brains exhibit increased self-renewal

activity in *HuD*−/− mice. Disruption of the *HuD* gene had similar positive effects on the cellular P behavior of the neural progenitor/stem cells derived from these three regions.

Discussion

Interestingly, we found that the ratio of neuron-producing neurospheres is decreased in *HuD*−/− mice. This could be interpreted as suggesting that HuD is required for (*i*) neuronal commitment of neural stem/progenitor cells, (*ii*) selective survival of neuronally committed progenitor cells, and/or (*iii*) production of postmitotic neurons from neuronal progenitor cells. The increased self-renewal activity of neural stem/progenitor cells observed in *HuD*−/− mice (Fig. 3) might lend the strongest support to the first possibility above. However, this issue should be investigated further in depth, because the latter two indicate the possible roles of HuD in committed neuronal progenitor cells. A previous study characterizing the expression of Hu proteins in subependymal zone cells of the adult songbird forebrain indicates that Hu proteins begin to be expressed in the neuronally committed progenitor cells only after the S phase, during either the premitotic G_2 phase of the progenitor cells or the early G_0/G_1 phase of the daughter cells (26). Furthermore, it was reported that *HuD* mRNA was expressed mainly in the intermediate and outer ventricular zones of the cortex, rather than in the cortical plate in E14.5 mice (4). In the spinal cord of stage 17 chick embryos, *HuD* mRNA was shown to be mainly localized in the ventral immature neuronal progeny, where the immunoreactivity of the 16A11(HuB/HuC/HuD) monoclonal antibody has not yet been seen (27). Taken together, it might be feasible to suggest that HuD commences its expression in proliferative neuronal progenitor cells and drives them to exit the mitotic cycle. We also found that the percentage of spheres that generate oligodendrocytes and astrocytes was not significantly changed in *HuD*−/− mice, indicating that HuD may not be involved in glial cell fate determination, and that its roles may be restricted to only the neuronally committed lineage.

The transcripts of p27 and p21, both cyclin-dependent kinase (CDK) inhibitors, have been reported as the binding targets of the Hu proteins. They are known to be involved in the acquisition of postmitotic phenotypes in the cells of neuronal lineages. Although overexpression of the Hu proteins in SH-SY5Y or PC12 cells induced the expression of CDK inhibitor proteins and growth arrest (W.A. and H.O., unpublished results), we could not detect any differences in the expression patterns or expression levels of the CDK inhibitors between *HuD*−/− mice and their wild-type littermates. It should be further investigated whether they are regulated by the Hu proteins and induce cell cycle exit of neuronal progenitors *in vivo*. Although HuD seems to be down-regulated in postmitotic mature neurons, it might still be required for the acquisition of the fully differentiated characteristics and various functions of mature neurons, including neurite extension and expression of neuronal markers. The mRNA of several neuronal proteins, including tau, GAP-43, and Neuroserpin, which are involved in the structure (e.g., neurite extension) and function of neurons, has also been reported to bind between their mRNA and Hu proteins (9, 10, 28). In this *HuD*−/− model, we examined the expression of GAP-43 and p27 protein by immunoblotting (Fig. 9, which is published as supporting information on the PNAS web site). We also examined the expression of tau mRNA by using real-time quantitive PCR in E17 brain (data not shown). Although we could not detect any significant difference in the expression of these molecules between *HuD*+/+ and *HuD*−/− mice, our observations do not directly deny the previous results of the study on GAP-43, p27, and tau. Even if not up-regulated, other Hu protein might have compensated the loss of *HuD* because of the functional redundancy of Hu-family proteins. Impaired cranial nerve development phenotype in E10.5 embryos (Fig. 2 *A–D*), impaired rotarod performance (Fig. 2*G*), and abnormal clasping reflex in the *HuD*−/− mice might lend support to such possibilities.

Conclusion

Based on the present loss-of-function studies, we suggest that HuD may be involved at multiple stages during neuronal development: (*i*) HuD negatively regulates the proliferation of neural stem/progenitor cells, (*ii*) HuD promotes the exit of neuronally committed progenitor cells from the cell cycle, and (*iii*) HuD promotes the differentiation of postmitotic neurons. It is of note that although the time of onset of the expression is, to some extent at least, specific for each of the HuB/C/D proteins (4), members of the Hu-family proteins showed marked similarities in their primary structures, expression profiles, and functions, as revealed by their misexpression studies. Thus, partially redundant functions of the different Hu proteins might mask the actual phenotype of the *HuD*-deficient mice in a developmental-stage-dependent manner (Fig. 2). Because our *HuD*-deficient mice were generated by an irremovable PGK-neocassette, and we cannot completely exclude the altered expression of neighborhood genes (29), future studies of multiple and conditional targeted disruptions using Cre-loxP system with a reversible neocassette may reveal the *in vivo* functions of Hu proteins in greater detail.

We thank Dr. Shin-ichiro Imai for technical assistance and helpful comments and Drs. Noriko Osumi, Takuya Shimazaki, and Kazunobu Sawamoto and members of the Okano laboratory for valuable discussions. This work was supported by grants from the Japanese Ministry of Education, Sports and Culture of Japan (to H.O.) and by a grant from the 21st Century Centers of Excellence Program of the Ministry of Education, Science and Culture of Japan (to Keio University).

1. Szabo, A., Dalmau, J., Manley, G., Rosenfeld, M., Wong, E., Henson, J., Posner, J. B. & Furneaux, H. M. (1991) *Cell* **67,** 325–333.
2. Ma, W. J., Cheng, S., Campbell, C., Wright, A. & Furneaux, H. (1996) *J. Biol. Chem.* **271,** 8144–8151.
3. Levine, T. D., Gao, F., King, P. H., Andrews, L. G. & Keene, J. D. (1993) *Mol. Cell. Biol.* **13,** 3494–3504.
4. Okano, H. J. & Darnell, R. B. (1997) *J. Neurosci.* **17,** 3024–3037.
5. Joseph, B., Orlian, M. & Furneaux, H. (1998) *J. Biol. Chem.* **273,** 20511–20516.
6. Kullmann, M., Gopfert, U., Siewe, B. & Hengst, L. (2002) *Genes Dev.* **16,** 3087–3099.
7. Ross, R. A., Lazarova, D. L., Manley, G. T., Smitt, P. S., Spengler, B. A., Posner, J. B. & Biedler, J. L. (1997) *Eur. J. Cancer* **33,** 2071–2074.
8. Antic, D., Lu, N. & Keene, J. D. (1999) *Genes Dev.* **13,** 449–461.
9. Chung, S., Eckrich, M., Perrone-Bizzozero, N., Kohn, D. T. & Furneaux, H. (1997) *J. Biol. Chem.* **272,** 6593–6598.
10. Aranda-Abreu, G. E., Behar, L., Chung, S., Furneaux, H. & Ginzburg, I. (1999) *J. Neurosci.* **19,** 6907–6917.
11. Atlas, R., Behar, L., Elliott, E. & Ginzburg, I. (2004) *J. Neurochem.* **89,** 613–626.
12. Akamatsu, W., Okano, H. J., Osumi, N., Inoue, T., Nakamura, S., Sakakibara, S., Miura, M., Matsuo, N., Darnell, R. B. & Okano, H. (1999) *Proc. Natl. Acad. Sci. USA* **96,** 9885–9890.
13. Kasashima, K., Terashima, K., Yamamoto, K., Sakashita, E. & Sakamoto, H. (1999) *Genes Cells* **4,** 667–683.
14. Quattrone, A., Pascale, A., Nogues, X., Zhao, W., Gusev, P., Pacini, A. & Alkon, D. L. (2001) *Proc. Natl. Acad. Sci. USA* **98,** 11668–11673.
15. Sakakibara, S., Nakamura, Y., Yoshida, T., Shibata, S., Koike, M., Takano, H., Ueda, S., Uchiyama, Y., Noda, T. & Okano, H. (2002) *Proc. Natl. Acad. Sci. USA* **99,** 15194–15199.
16. Osumi, N., Hirota, A., Ohuchi, H., Nakafuku, M., Iimura, T., Kuratani, S., Fujiwara, M., Noji, S. & Eto, K. (1997) *Development (Cambridge, U.K.)* **124,** 2961–2972.
17. Hitoshi, S., Alexson, T., Tropepe, V., Donoviel, D., Elia, A. J., Nye, J. S., Conlon, R. A., Mak, T. W., Bernstein, A. & van der Kooy, D. (2002) *Genes Dev.* **16,** 846–858.
18. Reynolds, B. A. & Weiss, S. (1992) *Science* **255,** 1707–1710.
19. Takahashi, T., Nowakowski, R. S. & Caviness, V. S., Jr. (1996) *J. Neurosci.* **16,** 6183–6196.
20. Baquet, Z. C., Gorski, J. A. & Jones, K. R. (2004) *J. Neurosci.* **24,** 4250–4258.
21. Mangiarini, L., Sathasivam, K., Seller, M., Cozens, B., Harper, A., Hetherington, C., Lawton, M., Trottier, Y., Lehrach, H., Davies, S. W., *et al.* (1996) *Cell* **87,** 493–506.
22. Takahashi, T., Nowakowski, R. S. & Caviness, V. S., Jr. (1997) *Dev. Neurosci.* **19,** 17–22.
23. Groszer, M., Erickson, R., Scripture-Adams, D. D., Lesche, R., Trumpp, A., Zack, J. A., Kornblum, H. I., Liu, X. & Wu, H. (2001) *Science* **294,** 2186–2189.
24. Nakayama, K., Ishida, N., Shirane, M., Inomata, A., Inoue, T., Shishido, N., Horii, I. & Loh, D. Y. (1996) *Cell* **85,** 707–720.
25. Morshead, C. M., Reynolds, B. A., Craig, C. G., McBurney, M. W., Staines, W. A., Morassutti, D., Weiss, S. & van der Kooy, D. (1994) *Neuron* **13,** 1071–1082.
26. Barami, K., Iversen, K., Furneaux, H. & Goldman, S. A. (1995) *J. Neurobiol.* **28,** 82–101.
27. Wakamatsu, Y. & Weston, J. A. (1997) *Development (Cambridge, U.K.)* **124,** 3449–3460.
28. Cuadrado, A., Garcia-Fernandez, L. F., Imai, T., Okano, H. & Munoz, A. (2002) *Mol. Cell Neurosci.* **20,** 198–210.
29. Olson, E. N., Arnold, H. H., Rigby, P. W. & Wold, B. J. (1996) *Cell* **85,** 1–4.

Available online at www.sciencedirect.com
SCIENCE DIRECT
Experimental Cell Research 306 (2005) 349–356
Experimental Cell Research
www.elsevier.com/locate/yexcr

Review

Function of RNA-binding protein Musashi-1 in stem cells☆

Hideyuki Okano*, Hironori Kawahara, Masako Toriya, Keio Nakao, Shinsuke Shibata, Takao Imai

Department of Physiology, Keio University School of Medicine, 35 Shinanomachi, Shinjuku-ku, Tokyo 160-8582, Japan

Received 26 January 2005, revised version received 21 February 2005
Available online 24 March 2005

Abstract

Musashi is an evolutionarily conserved family of RNA-binding proteins that is preferentially expressed in the nervous system. The first member of the Musashi family was identified in *Drosophila*. This protein plays an essential role in regulating the asymmetric cell division of ectodermal precursor cells known as sensory organ precursor cells through the translational regulation of target mRNA. In the CNS of *Drosophila* larvae, however, Musashi is expressed in proliferating neuroblasts and likely has a different function. Its probable mammalian homologue, Musashi-1, is a neural RNA-binding protein that is strongly expressed in fetal and adult neural stem cells (NSCs). Mammalian Musashi-1 augments Notch signaling through the translational repression of its target mRNA, m-Numb, thereby contributing to the self-renewal of NSCs. In addition to its functions in NSCs, the role of mammalian Musashi-1 protein in epithelial stem cells, including intestinal and mammary gland stem cells, is attracting increasing interest.

Keywords: Musashi; Translational regulation; Neural stem cell; Intestinal stem cell; Mammary gland stem cell; Notch signaling; Numb

Contents

Introduction

Neural stem cells (NSCs) are deserving of attention in terms of strategies for central nervous system (CNS) regeneration, but what kind of cells are they? NSCs are the organ (tissue) stem cells that reside in the organs (tissues) that are referred to as the CNS. Tissue stem cells are undifferentiated cells found in many adult tissues and possess certain fundamental properties in common, including multipotency (the ability to differentiate into the various cells that compose tissues), ability to self-renew, and ability to repair damaged tissue. The evidence regarding tissue stem cells obtained thus far suggests that in besides being present in the hematopoietic system, stem cells or stem-cell-like cells are present in the liver, intestine, mammary gland, testis, skeletal muscle, skin, hair follicles, myocardium, and neural crest-derived tissue, as well as in the CNS [1]. It is

☆ Invited minireview on a special issue "Molecular control of cellular differentiation".

* Corresponding author. Fax: +81 3 3357 5445.
E-mail address: hidokano@sc.itc.keio.ac.jp (H. Okano).

0014-4827/$ - see front matter © 2005 Elsevier Inc. All rights reserved.
doi:10.1016/j.yexcr.2005.02.021

surprising and very interesting that tissue stem cells are not only present in the hematopoietic system, intestine, and skin, which have rapid physiological cell turnover rates, but also in organs with slow physiological cell turnover rates that would be expected to have extremely poor ability to regenerate, including CNS.

NSCs are the tissue stem cells that are present in the CNS, and they can be defined conceptually as cells that possess a combination of multipotency and ability to self-renew. Great strides have been made in research on NSCs during approximately the past 10 years, and the main driving force behind this progress seems to have been the development of (i) a group of selective marker molecules for neural stem/progenitor cells, (ii) selective culture methods for NSCs, and (iii) methods for prospective identification and isolation of NSCs. We will leave detailed overall explanations of each of them to review articles [2–4] and the corresponding original articles, but our research group takes pride in the fact that we have made major contributions to the development of neural stem cell research tools. Although it is impossible to strictly discriminate between NSCs and progenitor cells based on whether they express a group of selective neural stem/progenitor cell marker molecules, a great deal of circumstantial evidence has indicated that the level of expression of the RNA-binding protein Musashi-1 [5–7], the intermediate filament Nestin [8,9], and the transcription factor Sox (*S*RY-like HMG b*ox*)-family molecules [10] is selectively higher in NSCs than in neural precursor cells. These properties can be exploited to enable live monitoring of neural stem cell activity and prospective identification and isolation of NSCs by means of reporter genes made to express green fluorescence protein (GFP) by using the promoter or enhancer region of this group of genes [11]. In the present study, we would like to describe the process that led to the discovery of the neural stem/progenitor cell marker Musashi-1, which is regarded as having greatly contributed to stem-cell biology, not only as a marker, but because it has provided insights into the role of post-transcriptional gene regulation in the maintenance of stem cells.

Discovery and analysis of the function of the Drosophila MUSASHI gene

Musashi-1 is an RNA-binding protein family that is strongly expressed in the nervous system [12] and whose primary structure and expression pattern have been conserved among species in nematodes (*C. elegans*) [13], the fruit fly (*Drosophila*) [14,15], ascidians (*Ciona intestinalis*) [16], and in vertebrates as a whole [5,17]. Based on the loss-of-function phenotypes of the *musashi* gene in *Drosophila*, this gene was shown to play an essential role in the for asymmetrical division of sensory organ precursor cells (SOPs), which are precursor cells of the ectodermal system that are common to both neural and non-neural cell lineages. In wild-type *Drosophila*, each SOP normally gives rise to one IIa cell (non-neural precursor), which is an intermediate precursor cell, and one IIb cell (neural precursor), whereas in *musashi* mutants, SOPs are incapable of dividing asymmetrically, and two IIa cells are produced instead. As a result, the neural lineage derived from IIb cells that originally should have produced neural cells, such as neurons and glia, undergoes phenotypic transformation to hair-forming cells and socket-forming cells as support cells, which are IIa-cell-derived non-neural lineage cells, resulting in double-bristle phenotype with two hairs. The name MUSASHI, which refers to "bearing two swords", is derived from this double-bristle phenotype [12,14,18].

We were later able to clarify the regulatory mechanism of the asymmetric cell division of SOPs by the Musashi gene product of *Drosophila*. Starting with the conclusion, the Musashi gene product, which is an RNA-binding protein, was found to induce differentiation of IIb cells as neural precursor cells by selectively repressing translation of the mRNA of the neural differentiation inhibitory factor (a transcription repressor possessing a BTB domain and zinc-finger domain) called Tramtrack69 (TTK69) in IIb cells alone. In other words, although transcription of the *ttk69* gene actually occurs with similar efficiency in both IIa cells and IIb cells, translation of its mRNA in IIb cells is repressed by Musashi protein. TTK69 protein is expressed in IIa cells alone, and as a result it represses differentiation of IIa cells into neural precursor cells. The discovery that modulation of gene expression at the translation level regulates asymmetrical division is considered extremely interesting. However, in the early 1990s, when identification of the *musashi* gene was first reported, functional analysis of RNA-binding proteins had not yet been established. Identification of the RNA sequence and gene that was the target of the Musashi protein was absolutely essential to achieving a breakthrough. After spending several years establishing the conditions, we succeeded in identifying the RNA base sequence that is the binding-target of Musashi protein, which possesses two RNA-binding motifs, by using the in vitro selection method (SELEX method). More specifically, we chemically synthesized a DNA template (5′-GGGAAGATCTCGACCAGAAG-N_{50}-TATGTG-CGTCTACATGGATCCTCA-3′) with the T7 RNA polymerase recognition sequence attached at the 5′ end of a random DNA oligomer and the primer sequence for the reverse transcription by reverse polymerase at the 3′ end, and then prepared random-sequence RNA (random RNA pool) in a test tube by adding T7 RNA polymerase. Then, we added purified GST–Musashi fusion protein to a random RNA pool, and used a Glutathione–Sepharose 4Bs affinity column to isolate only the RNA molecule that binds to the GST–Musashi fusion protein. We later synthesized the corresponding cDNA by reverse transcription, amplified it by PCR between the T7 RNA polymerase recognition sequence and the primer sequence for reverse transcription, and then prepared template DNA for RNA synthesis. When this cycle was repeated 5 times, the RNA molecule that binds to the GST–Musashi fusion protein was highly